9

Quarkonium mesons in strongly coupled plasma

As discussed in Section 2.4, heavy quarks and quarkonium mesons, with masses such that $M/T \gg 1$, constitute valuable probes of the QGP. Since dynamical questions about these probes are very hard to answer from first principles, here we will study analogous questions in the strongly coupled $\mathcal{N} = 4$ SYM plasma. In this case the gauge/string duality provides the tool that makes a theoretical treatment possible. Although for concreteness we will focus on the $\mathcal{N} = 4$ plasma, many of the results that we will obtain are rather universal in the sense that, at least qualitatively, they hold for any strongly coupled gauge theory with a string dual. Such results may give us insights relevant for the QCD quark–gluon plasma at temperatures at which it is reasonably strongly coupled.

The QGP only exists at temperatures $T > T_c$, so in QCD the condition $M/T \gg 1$ can only be realized by taking M to be large. In contrast, $\mathcal{N} = 4$ SYM is a conformal theory with no confining phase, so all temperatures are equivalent. In the presence of an additional scale, namely the quark or the meson mass, the physics only depends on the ratio M/T. This means that in the $\mathcal{N} = 4$ theory the condition $M/T \gg 1$ can be realized by fixing T and sending M to infinity, or by fixing M and sending $T \to 0$; both limits are completely equivalent. In particular, the leading order approximation to the heavy quark or quarkonium meson physics, in an expansion in T/M, may be obtained by setting $T = 0$. For this reason, this is the limit that we will study first.

We will follow the nomenclature common in the QCD literature and refer to mesons made of two heavy quarks as "quarkonium mesons" or "quarkonia", as opposed to using the term "heavy mesons", which commonly encompasses mesons made of one heavy and one light quark.

9.1 Adding quarks to $\mathcal{N} = 4$ SYM

In Section 5.5 we saw that N_f flavors of fundamental matter can be added to $\mathcal{N} = 4$ SYM by introducing N_f D7-brane probes into the geometry sourced by

https://doi.org/10.1017/9781009403504.009 Published online by Cambridge University Press

the D3-branes, as indicated by the array (5.98), which we reproduce here (with the time direction included) for convenience:

$$\begin{array}{lcccccccccc} \text{D3:} & 0 & 1 & 2 & 3 & \_ & \_ & \_ & \_ & \_ & \_ \\ \text{D7:} & 0 & 1 & 2 & 3 & 4 & 5 & 6 & 7 & \_ & \_ \end{array} \quad . \tag{9.1}$$

Before we proceed, let us clarify an important point. $\mathcal{N} = 4$ SYM is a conformal theory, i.e. its β-function vanishes exactly. Adding matter to it, even if the matter is massless, makes the quantum mechanical β-function positive, at least perturbatively. This means that the theory develops a Landau pole in the UV and is therefore not well defined at arbitrarily high energy scales.[1] However, since the β-function (for the 't Hooft coupling λ) is proportional to N_f/N_c, the Landau pole occurs at a scale of order e^{N_c/N_f}. This is exponentially large in the limit of interest here, $N_f/N_c \ll 1$, and in fact the Landau pole disappears altogether in the strict probe limit $N_f/N_c \to 0$. On the string side, the potential pathology associated with a Landau pole manifests itself in the fact that a completely smooth solution that incorporates the backreaction of the D7-branes may not exist [28, 383, 223, 535, 136, 320]. In any case, the possible existence of a Landau pole at high energies will not be of concern for the applications reviewed here. In the gauge theory, it will not prevent us from extracting interesting infrared physics, just as the existence of a Landau pole in QED does not prevent one from calculating the conductivity of an electromagnetic plasma. In the string description, we will not go beyond the probe approximation, so the backreaction of the D7-branes will not be an issue.[2] And finally, we note that we will work with the D3/D7 model because of its simplicity. We could work with a more sophisticated model with better UV properties, but this would make the calculations more involved while leaving the physics we are interested in essentially unchanged.

As illustrated in Fig. 9.1, the D3-branes and the D7-branes can be separated a distance L in the 89-directions. This distance times the string tension, Eq. (4.11), is the minimum energy of a string stretching between the D3-branes and the D7-branes. Since the quarks arise as the lightest modes of these 3–7 strings, this energy is precisely the bare quark mass:

$$M_{\rm q} = \frac{L}{2\pi\alpha'} \,. \tag{9.2}$$

An important remark here is the fact that the branes in Fig. 9.1 are implicitly assumed to be embedded in flat spacetime. In Section 5.5 this was referred to as the "first" or "open string" description of the D3/D7 system, which is reliable in the regime $g_s N_c \ll 1$, in which the backreaction of the D3-branes on spacetime can be

[1] Nonperturbatively, the possibility that a strongly coupled fixed point exists must be ruled out before reaching this conclusion. See [320] for an argument in this direction based on supersymmetry.

[2] For a review of 'unquenched' models, i.e. those in which the flavor backreaction is included, see [659].

https://doi.org/10.1017/9781009403504.009 Published online by Cambridge University Press

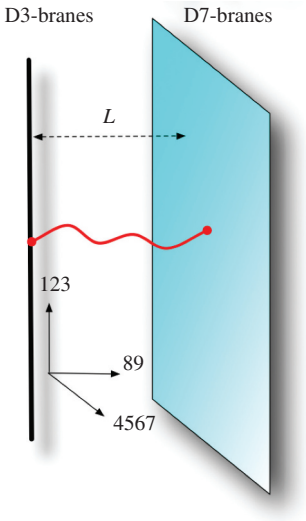

Figure 9.1 D3/D7 system at weak coupling, with a string (red) stretching between the D3-branes and D7-branes.

ignored. One of our main tasks in the following Sections will be to understand how this picture is modified in the opposite regime, $g_s N_c \gg 1$, when the D3-branes are replaced by their backreaction on spacetime. In this regime the shape of the D7-branes may or may not be modified, but Eq. (9.2) will remain true provided the appropriate definition of L, to be given below, is used.

Although $\mathcal{N} = 4$ SYM is a conformal theory, the addition of quarks with a nonzero mass introduces a scale and gives rise to a rich spectrum of quark–antiquark bound states, i.e. mesons. In the following section we will study the meson spectrum in this theory at zero temperature in the regime of strong 't Hooft coupling, $g_s N_c \gg 1$. On the gauge theory side this is inaccessible to conventional methods such as perturbation theory, but on the string side a classical description in terms of D7-brane probes in a weakly curved $\mathrm{AdS}_5 \times S^5$ applies. Our first task is thus to understand in more detail the way in which the D7-branes are embedded in this geometry. Since this is crucial for subsequent sections, we will in fact provide a fair amount of detail here.

9.2 Zero temperature

9.2.1 D7-brane embeddings

We begin by recalling that the coordinates in the $\mathrm{AdS}_5 \times S^5$ metric (5.1), (5.2) can be understood as follows. The four directions t, x_i correspond to the 0123-directions in (9.1). The 456789-directions in the space transverse to the D3-branes give rise to the radial coordinate r in AdS_5, defined through

https://doi.org/10.1017/9781009403504.009 Published online by Cambridge University Press

$$r^2 = x_4^2 + \cdots + x_9^2 \,, \tag{9.3}$$

as well as five angles that parametrize the S^5. We emphasize that, once the gravitational effect of the D3-branes is taken into account, the six-dimensional space transverse to the D3-branes is not flat, so the $x^4, \ldots, x^9$ coordinates are not Cartesian coordinates. However, they are still useful to label the different directions in this space.

The D7-branes share the 0123-directions with the D3-branes, so from now on we will mainly focus on the remaining directions. In the six-dimensional space transverse to the D3-branes, the D7-branes span only a four-dimensional subspace parametrized by $x_4, \ldots, x_7$. Since the D7-branes preserve the $SO(4)$ rotational symmetry in this space, it is convenient to introduce a radial coordinate u such that

$$u^2 = x_4^2 + \cdots + x_7^2 \,, \tag{9.4}$$

as well as three spherical coordinates, denoted collectively by Ω_3, that parametrize an S^3. Similarly, it is useful to introduce a radial coordinate U in the 89-plane through

$$U = x_8^2 + x_9^2 \,, \tag{9.5}$$

as well as a polar angle α. In terms of these coordinates one has

$$dx_4^2 + \cdots + dx_9^2 = du^2 + u^2 d\Omega_3^2 + dU^2 + U^2 d\alpha^2 \,. \tag{9.6}$$

Obviously, the overall radial coordinate r satisfies $r^2 = u^2 + U^2$.

Since the D7-branes only span the 4567-directions, they only wrap an S^3 inside the S^5. The D7-brane worldvolume may thus be parametrized by the coordinates $\{t, x_i, u, \Omega_3\}$. In order to specify the D7-branes' embedding one must then specify the remaining spacetime coordinates, U and α, as functions of, in principle, all the worldvolume coordinates. However, translational symmetry in the $\{t, x_i\}$-directions and rotational symmetry in the $\{\Omega_3\}$-directions allow U and α to depend only on u.

In order to understand this dependence, consider first the case in which the spacetime curvature generated by the D3-branes is ignored. In this case, the D7-branes lie at a constant position in the 89-plane, see Fig. 9.2. In other words, their embedding is given by $\alpha(u) = \alpha_0$ and $U(u) = L$, where α_0 and L are constants. The first equation can be understood as saying that, because of the $U(1)$ rotational symmetry in the 89-plane, the D7-branes can sit at any constant angular position; choosing α_0 then breaks the symmetry. Since this $U(1)$ symmetry is respected by the D3-branes' backreaction (i.e. since the $AdS_5 \times S^5$ metric is $U(1)$-invariant), it is easy to guess (correctly) that $\alpha(u) = \alpha_0$ is still a solution of the D7-branes' equation of motion in the presence of the D3-branes' backreaction.

https://doi.org/10.1017/9781009403504.009 Published online by Cambridge University Press

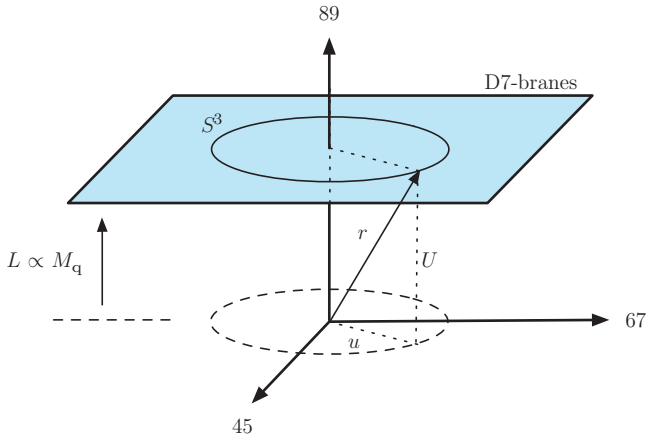

Figure 9.2 Coordinates in the six-dimensional space transverse to the D3-branes. Each axis actually represents two directions, i.e. a plane (or, equivalently, the radial direction in that plane). The asymptotic distance $L = U(u = \infty)$ is proportional to the quark mass, Eq. (9.2). We emphasize that the directions parallel to the D3-branes (the gauge theory directions t, x_i) are suppressed in this picture, and they should not be confused with the D7 directions shown in the figure, which lie entirely in the space transverse to the D3-branes.

The second equation, $U(u) = L$, says that the D7-branes lie at a constant distance from the D3-branes. In the absence of the D3-branes' backreaction this is easily understood: there is no force on the D7-branes and therefore they span a perfect 4-plane. In the presence of backreaction, one should generically expect that the spacetime curvature deforms the D7-branes as in Fig. 9.3, bending them towards the D3-branes at the origin. The reason that this does not happen for the D3/D7 system at zero temperature is that the underlying supersymmetry of the system guarantees an exact cancelation of forces on the D7-branes. In fact, it is easy to verify directly that $U(u) = L$ is still an exact solution of the D7-branes' equations of motion in the presence of the D3-branes' backreaction. The constant L then determines the quark mass through Eq. (9.2). We will see below that the introduction of nonzero temperature breaks supersymmetry completely, and that consequently $U(u)$ becomes a non-constant function that one must solve for, and that this function contains information about the ground state of the theory in the presence of quarks. For example, its asymptotic behavior encodes the value of the bare quark mass M_q and the quark condensate $\langle\bar{\psi}\psi\rangle$, whereas its value at $u = 0$ is related to the quark thermal mass M_{th}. Since in this section we work at $T = 0$, any nonzero quark mass corresponds to $M_q/T \to \infty$. In this sense one must think of the quarks in question as the analog of heavy quarks in QCD, and of the quark condensate as the analog of $\langle\bar{c}c\rangle$ or $\langle\bar{b}b\rangle$. However, when we consider a nonzero temperature in subsequent Sections, whether the holographic quarks described by

https://doi.org/10.1017/9781009403504.009 Published online by Cambridge University Press

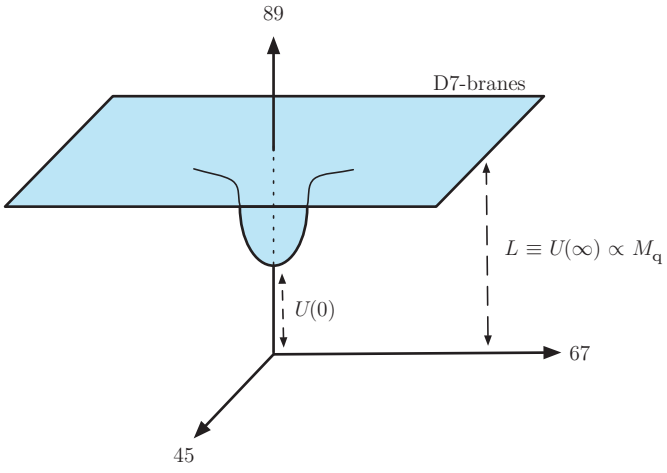

Figure 9.3 Possible bending of the D7-branes at nonzero temperature. The asymptotic distance $L \equiv U(\infty)$ is proportional to the bare quark mass $M_{\rm q}$, whereas the minimum distance $U(0)$ is related (albeit in a way more complicated than simple proportionality) to the quark thermal mass.

the D7-branes are the analogs of heavy or light quarks in QCD will depend on how their mass (or, more precisely, the mass of the corresponding mesons) compares to the temperature.

We have concluded that, at zero temperature, the D7-branes lie at $U = L$ and are parametrized by $\{t, x_i, u, \Omega_3\}$. In terms of these coordinates, the metric induced on the D7-branes by the metric (5.1)–(5.2) for the $AdS_5 \times S^5$ spacetime takes the form

$$ds^2 = \frac{u^2 + L^2}{R^2}\left(-dt^2 + dx_i^2\right) + \frac{R^2}{u^2 + L^2}du^2 + \frac{R^2 u^2}{u^2 + L^2}d\Omega_3^2 \,. \qquad (9.7)$$

We see that if $L = 0$ then this metric is exactly that of $AdS_5 \times S^3$. The AdS_5 factor suggests that the dual gauge theory should still be conformally invariant. This is indeed the case in the limit under consideration: If $L = 0$ the quarks are massless and the theory is classically conformal, and in the probe limit $N_f/N_c \to 0$ the quantum mechanical β-function, which is proportional to N_f/N_c, vanishes. If $L \neq 0$ then the metric above becomes $AdS_5 \times S^3$ only asymptotically, i.e. for $u \gg L$, reflecting the fact that in the gauge theory conformal invariance is explicitly broken by the quark mass $M_{\rm q} \propto L$, but is restored asymptotically at energies $E \gg M_{\rm q}$. We also note that, if $L \neq 0$, then the radius of the three-sphere is not constant, as displayed in Fig. 9.4; in particular, it shrinks to zero at $u = 0$ (corresponding to $r = L$), at which point the D7-branes "terminate" from the viewpoint of the projection on AdS_5 [513]. In other words, if $L \neq 0$ then the D7-branes fill the AdS_5 factor of the metric only down to a minimum value of the radial direction

https://doi.org/10.1017/9781009403504.009 Published online by Cambridge University Press

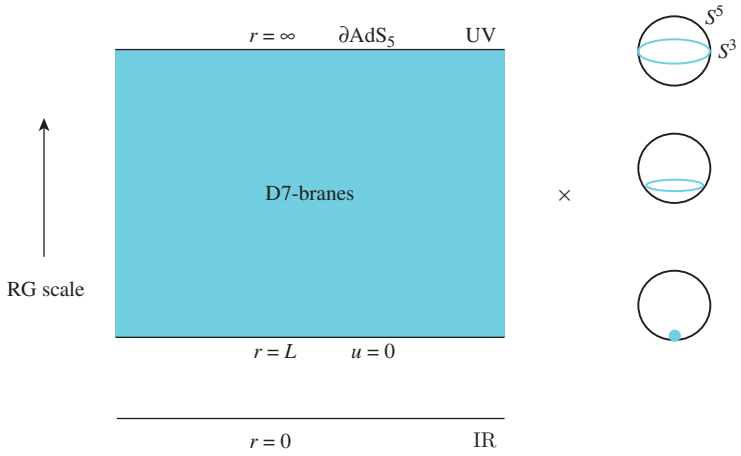

Figure 9.4 D7-branes' embedding in $AdS_5 \times S^5$. At nonzero temperature this picture is slightly modified. First, a horizon appears at $r = r_0 > 0$, and second, the D7-branes terminate at $r = U(0) < L$. This "termination point" corresponds to the tip of the branes in Fig. 9.3.

proportional to the quark mass. As we anticipated above, at nonzero temperature one must distinguish between the bare and the thermal quark masses, related to $U(\infty)$ and $U(0)$ respectively. In this case the position in AdS at which the D7-branes terminate is $r = U(0) < L$, and therefore they fill the AdS space down to a radial position related to the thermal mass. Note also that at finite temperature a horizon is present at $r = r_0 > 0$.

9.2.2 Meson spectrum

We are now ready to compute the spectrum of low spin mesons in the D3/D7 system following Ref. [559]. The spectrum for more general Dp/Dq systems was computed in [60, 637, 704]. Recall that mesons are described by open strings attached to the D7-branes. In particular, spin zero and spin one mesons correspond to the scalar and vector fields on the D7-branes. Large spin mesons can be described as long, semi-classical strings [559, 561, 666, 673, 301, 674, 116, 159, 668, 44], but we will not review them here.

For simplicity, we will focus on scalar mesons. Following Section 5.1.5, we know that in order to determine the spectrum of scalar mesons, we need to determine the spectrum of normalizable modes of small fluctuations of the scalar fields on the D7-branes. At this point we restrict ourselves to a single D7-brane, i.e. we set $N_f = 1$, in which case the dynamics is described by the DBI action (4.18). At leading order in the large-N_c expansion, the spectrum for $N_f > 1$ consists of N_f^2 identical copies of the single-flavor spectrum [560].

https://doi.org/10.1017/9781009403504.009 Published online by Cambridge University Press

We use the coordinates in Eq. (9.7) as worldvolume coordinates for the D7-brane, which we collectively denote by σ^μ. The physical scalar fields on the D7-brane are then $x^8(\sigma^\mu)$, $x^9(\sigma^\mu)$. By a rotation in the 89-plane we can assume that, in the absence of fluctuations, the D7-brane lies at $x^8 = 0$, $x^9 = L$. Then the fluctuations can be parametrized as

$$x^8 = 0 + \varphi(\sigma^\mu) \,, \qquad x^9 = L + \tilde{\varphi}(\sigma^\mu) \,, \tag{9.8}$$

with φ and $\tilde{\varphi}$ the scalar fluctuations around the fiducial embedding. In order to determine the normalisable modes, it suffices to work to quadratic order in $\varphi, \tilde{\varphi}$. Substituting (9.8) in the DBI action (4.18) and expanding in $\varphi, \tilde{\varphi}$ leads to a quadratic Lagrangian whose corresponding equation of motion is

$$\frac{R^4}{(u^2+L^2)^2}\Box\varphi + \frac{1}{u^3}\partial_u(u^3\partial_u\varphi) + \frac{1}{u^2}\nabla^2\varphi = 0 \,, \tag{9.9}$$

where $\Box$ is the four-dimensional d'Alembertian associated with the Cartesian coordinates t, x_i, and ∇^2 is the Laplacian on the three-sphere. The equation for $\tilde{\varphi}$ takes exactly the same form. Modes that transform non-trivially under rotations on the sphere correspond to mesons that carry nonzero R-charge. Since QCD does not possess an R-symmetry, we will restrict ourselves to R-neutral mesons, meaning that we will assume that φ does not depend on the coordinates of the sphere. We can use separation of variables to write these modes as

$$\varphi = \phi(u)e^{iq\cdot x} \,, \tag{9.10}$$

where $x = (t, x_i)$. Each of these modes then corresponds to a physical meson state in the gauge theory with a well defined four-dimensional mass given by its eigenvalue under $\Box$, that is, $M^2 = -q^2$. For each of these modes, Eq. (9.9) results in an equation for $\phi(u)$ that, after introducing dimensionless variables through

$$\bar{u} = \frac{u}{L} \,, \qquad \bar{M}^2 = -\frac{k^2R^4}{L^2} \,, \tag{9.11}$$

becomes

$$\partial_{\bar{u}}^2\phi + \frac{3}{\bar{u}}\,\partial_{\bar{u}}\phi + \frac{\bar{M}^2}{(1+\bar{u}^2)^2}\,\phi = 0 \,. \tag{9.12}$$

This equation can be solved in terms of hypergeometric functions. The details can be found in Ref. [559], but we will not give them here because most of the relevant physics can be extracted as follows.

Equation (9.12) is a second order, ordinary differential equation with two independent solutions. The combination we seek must satisfy two conditions: It must be normalizable as $\bar{u} \to \infty$, and it must be regular as $\bar{u} \to 0$. For arbitrary values

https://doi.org/10.1017/9781009403504.009 Published online by Cambridge University Press

of $\bar{M}$, both conditions cannot be simultaneously satisfied. In other words, the values of $\bar{M}$ for which physically acceptable solutions exist are quantised. Since Eq. (9.12) contains no dimensionful parameters, the values of $\bar{M}$ must be pure numbers. These can be explicitly determined from the solutions of (9.12) and they take the form [559]

$$\bar{M}^2 = 4(n+1)(n+2)\,, \qquad n = 0, 1, 2, \ldots. \tag{9.13}$$

Using this, and $M^2 = -q^2 = \bar{M}^2 L^2/R^4$, we derive the result that the four-dimensional mass spectrum of scalar mesons is

$$M(n) = \frac{2L}{R^2}\sqrt{(n+1)(n+2)} = \frac{4\pi M_{\rm q}}{\sqrt{\lambda}}\sqrt{(n+1)(n+2)}\,, \tag{9.14}$$

where in the last equality we have used the expressions $R^2/\alpha' = \sqrt{\lambda}$ and (9.2) to write R and L in terms of gauge theory parameters. We thus conclude that the spectrum consists of a discrete set of mesons with a mass gap given by the mass of the lightest meson:[3]

$$M_{\rm mes} = 4\pi\sqrt{2}\,\frac{M_{\rm q}}{\sqrt{\lambda}}\,. \tag{9.15}$$

Since this result is valid at large 't Hooft coupling, $\lambda \gg 1$, the mass of these mesons is much smaller than the mass of two constituent quarks. In other words, the mesons in this theory are very deeply bound. In fact, the binding energy

$$E_B \equiv 2M_{\rm q} - M_{\rm mes} \lesssim 2M_{\rm q} \sim \sqrt{\lambda} M_{\rm mes} \tag{9.16}$$

is so large that it almost cancels the rest energy of the quarks. This is clear from the gravity picture of "meson formation" (see Fig. 9.5), in which two strings of opposite orientation stretching from the D7-brane to $r = 0$ (the quark–antiquark pair) join together to form an open string with both ends on the D7-brane (the meson). This resulting string is much shorter than the initial ones, and hence corresponds to a configuration with much lower energy. This feature is an important difference with quarkonium mesons in QCD, such as charmonium or bottomonium, which are not deeply bound. Although this certainly means that caution must be exercised when trying to compare the physics of quarkonium mesons in holographic theories with the physics of quarkonium mesons in QCD, the success or failure of these comparisons cannot be assessed at this point. We will discuss this assessment in detail below, once we have learned more about the physics of holographic mesons. Suffice it to say here that some of this physics, such as the temperature or the velocity dependence of certain meson properties, turns out to be quite general

[3] In order to compare this and subsequent formulas with Ref. [559] and others, note that our definition (4.17) of g^2 differs from the definition in some of those references by a factor of 2, for example $g^2_{\rm [here]} = 2g^2_{\rm [559]}$.

https://doi.org/10.1017/9781009403504.009 Published online by Cambridge University Press

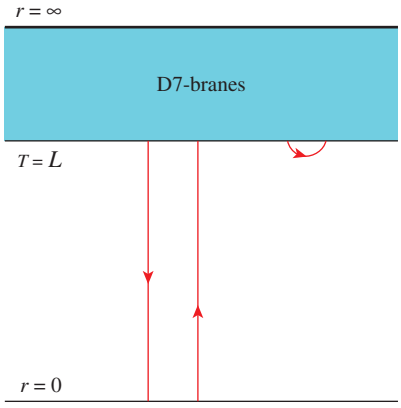

Figure 9.5 String description of a quark, an antiquark and a meson. The string that describes the meson can be much shorter than those describing the quark and the antiquark.

and may yield insights into some of the challenges related to understanding the physics of quarkonia within the QCD quark–gluon plasma.

We close this section with a consistency check. The behavior of the fluctuation modes at infinity is related to the high energy properties of the theory. At high energy, we can ignore the effect of the mass of the quarks and the theory becomes conformal. The $u \to \infty$ behavior is then related to the UV operator of the lowest conformal dimension, Δ, that has the same quantum numbers as the meson [392, 803]. Analysis of this behavior for the solutions of Eqs. (9.9) and (9.12) shows that $\Delta = 3$ [559], as expected for a quark-bilinear operator.

9.3 Nonzero temperature

9.3.1 D7-brane embeddings

We now turn to the case of nonzero temperature, $T \neq 0$. This means that we must study the physics of a D7-brane in the black brane metric (cf. Eq. (5.33))

$$ds^2 = \frac{r^2}{R^2}\left(-f dt^2 + dx_1^2 + dx_2^2 + dx_3^2\right) + \frac{R^2}{r^2 f} dr^2 + R^2 d\Omega_5^2 , \qquad (9.17)$$

where

$$f(r) = 1 - \frac{r_0^4}{r^4} , \qquad r_0 = \pi R^2 T . \qquad (9.18)$$

The study we must perform is conceptually analogous to that of the past few sections, but the equations are more involved and most of them must be solved numerically. These technical details are not very illuminating, and for this reason we will not dwell into them. Instead, we will focus on describing in detail the main

https://doi.org/10.1017/9781009403504.009 Published online by Cambridge University Press

conceptual points and results, as well as the physics behind them, which in fact can be understood in very simple and intuitive terms.

As mentioned above, at $T \neq 0$ all supersymmetry is broken. We therefore expect that the D7-branes will be deformed by the non-trivial geometry. In particular, the introduction of nonzero temperature corresponds, in the string description, to the introduction of a black brane in the background. Intuitively, we expect that the extra gravitational attraction will bend the D7-branes towards the black hole. This simple conclusion, which was anticipated in previous sections, has far-reaching consequences. At a qualitative level, most of the holographic physics of mesons in a strongly coupled plasma follows from this conclusion. An example of the D7-branes' embedding for a small value of $T/M_{\rm q}$ is depicted in two slightly different ways in Fig. 9.6.

The qualitative physics of the D3/D7 system as a function of the dimensionless ratio $T/M_{\rm q}$ is now easy to guess, and is captured by Fig. 9.7. At zero temperature the horizon has zero size and the D7-branes span an exact hyperplane. At nonzero but sufficiently small $T/M_{\rm q}$, the gravitational attraction from the black hole pulls the branes down but the branes' tension can still compensate for this. The embedding of the branes is thus deformed, but the branes remain entirely outside the horizon. Since in this case the induced metric on the D7-branes has no horizon, we will call this type of configuration a "Minkowski embedding". In contrast, above a critical temperature $T_{\rm diss}$,[4] the gravitational force overcomes the tension of the branes and these are pulled into the horzion. In this case the induced metric on the branes possesses an event horizon, inherited from that of the spacetime metric. For this reason we will refer to such configurations as "black hole embeddings". Between these two types of embeddings there exists a so-called critical embedding in which the branes just "touch the horizon at a point". The existence of such an interpolating solution might lead one to suspect that the phase transition between Minkowski and black hole embeddings is continuous, i.e. of second or higher order. However, as we will see in the next section, thermodynamic considerations reveal that a first order phase transition occurs between a Minkowski and a black hole embedding. In other words, the critical embedding is skipped over by the phase transition, and near-critical embeddings turn out to be metastable or unstable.

As illustrated by the figures above, the fact that the branes bend towards the horizon implies that the asymptotic distance between the two differs from their minimal distance. As we will see in Section 9.3.2, the asymptotic distance is proportional to the microscopic or "bare" quark mass, since it is determined by the non-normalizable mode of the field that describes the branes' bending. In contrast, the minimal distance between the branes and the horizon includes thermal (and

[4] The reason for the subscript will become clear shortly.

https://doi.org/10.1017/9781009403504.009 Published online by Cambridge University Press

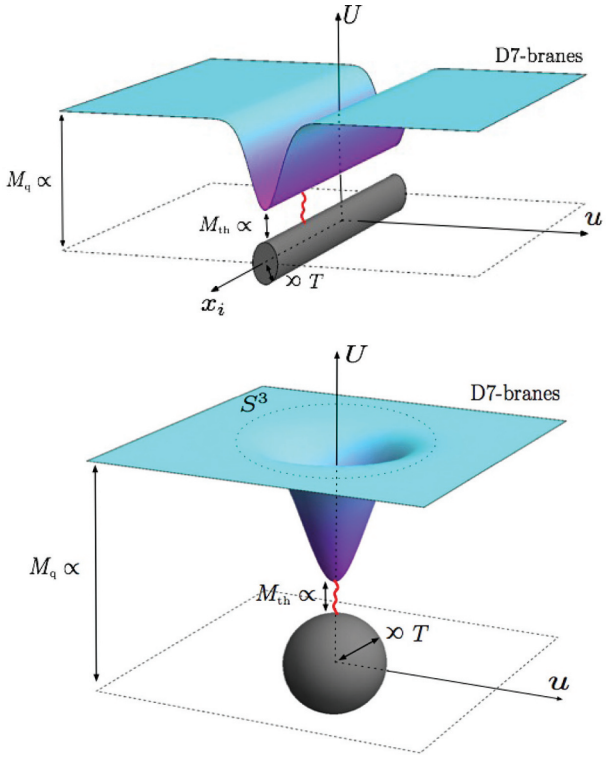

Figure 9.6 D7-branes' embedding for small T/M_q. The branes bend towards the horizon, shown in dark grey. The radius of the horizon is proportional to its Hawking temperature, which is identified with the gauge theory temperature T – see Eq. (9.18). The asymptotic position of the D7-branes is proportional to the bare quark mass, M_q. The minimum distance between the branes and the horizon is related to the thermal quark mass, because this is the minimum length of a string (shown as a red wiggly line) stretching between the branes and the horizon. The top figure shows the two relevant radial directions in the space transverse to the D3-branes, U and u (introduced in Eqs. (9.4) and (9.5)), together with the gauge theory directions x_i (time is suppressed). The horizon has topology $\mathbb{R}^3 \times S^5$, where the first factor corresponds to the gauge-theory directions. This "cylinder-like" topology is manifest in the top figure. Instead, in the bottom figure the gauge theory directions are suppressed and the S^3 wrapped by the D7-branes in the space transverse to the D3-branes is shown, as in Figs. 9.2 and 9.3. In this figure only the S^5 factor of the horizon is shown. Figure adapted from Ref. [256].

quantum) effects, and for this reason we will refer to the mass of a string stretching between the bottom of the branes and the horizon (shown as a wiggly red curve in the figures) as the "thermal" quark mass. Note that this vanishes in the black hole phase.

Although we will come back to this important point below, we wish to emphasize right from the start that the phase transition under discussion is *not* a confinement–deconfinement phase transition, since the presence of a black hole implies that both

https://doi.org/10.1017/9781009403504.009 Published online by Cambridge University Press

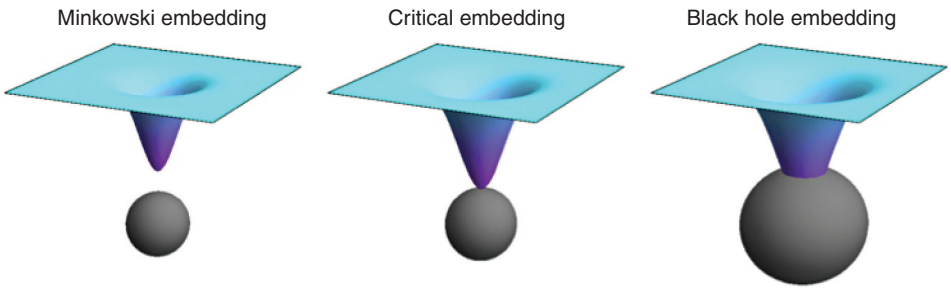

Figure 9.7 Various D7-brane configurations in a black D3-brane background with increasing temperature from left to right. At low temperatures, the probe branes close off smoothly above the horizon. At high temperatures, the branes fall through the event horizon. In between, a critical solution exists in which the branes just "touch" the horizon at a point. The critical configuration is never realized: a first order phase transition occurs from a Minkowski to a black hole embedding (or vice versa) before the critical solution is reached. Figure adapted from Ref. [256].

phases are deconfined. Instead, we will see that the branes' phase transition corresponds to the *dissociation* of heavy quarkonium mesons. In order to illustrate the difference most clearly, consider first a holographic model of a confining theory, as described in Section 5.2.2; below we will come back to the case of $\mathcal{N} = 4$ SYM. For all such confining models, the difference between the deconfinement and the dissociation phase transitions is illustrated in Fig. 9.8. Below T_c, the theory is in a confining phase and therefore no black hole is present. At some T_c, a deconfinement transition takes place, which in the string description corresponds to the appearance of a black hole whose size is proportional to T_c. If the quark mass is sufficiently large compared to T_c then the branes remain outside the horizon (top part of the figure); otherwise they fall through the horizon (bottom part of the figure). The first case corresponds to heavy quarkonium mesons that remain bound in the deconfined phase, and that eventually dissociate at some higher $T_{\rm diss} > T_c$. The second case describes light mesons that dissociate as soon as the deconfinement transition takes place.

Figure 9.8 also applies to $\mathcal{N} = 4$ SYM theory with $T_c = 0$ in the sense that, although the vacuum of the theory is not confining, there is no black hole at $T = 0$. Note also that mesons only exist provided $M_{\rm q} > 0$, since otherwise the theory is conformal and there is no particle spectrum. This means that in $\mathcal{N} = 4$ SYM theory any meson is a heavy quarkonium meson that remains bound for some range of temperatures above $T_c = 0$, as described by the top part of Fig. 9.8. In the case $M_{\rm q} = 0$ we cannot properly speak of mesons, but we see that the situation is still described by the bottom part of the figure in the sense that in this case the branes fall through the horizon as soon as T is raised above $T_c = 0$.

https://doi.org/10.1017/9781009403504.009 Published online by Cambridge University Press

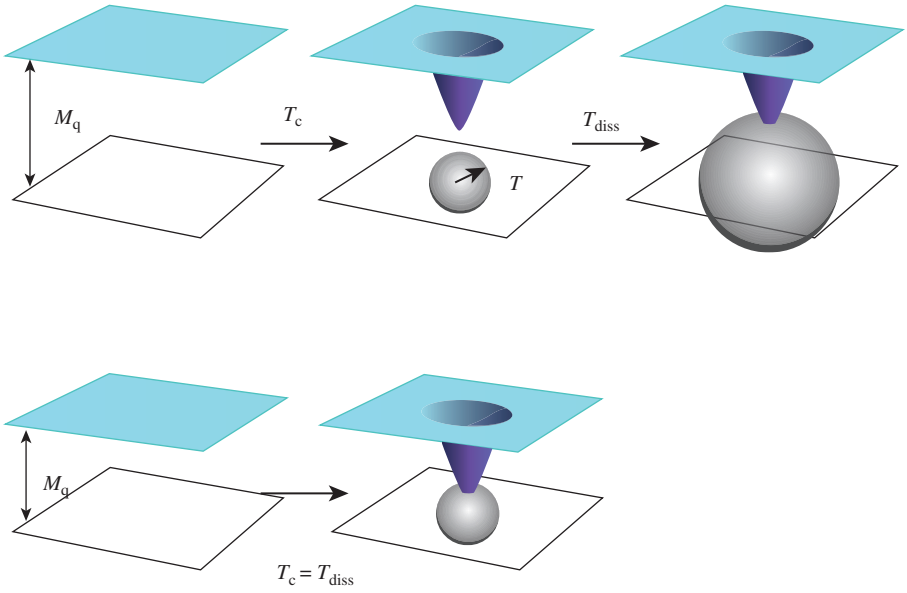

Figure 9.8 Top: sufficiently heavy quarkonium mesons remain bound in the deconfined phase (above T_c) and dissociate at $T_{diss} > T_c$. Bottom: in contrast, light mesons dissociate as soon as the deconfinement phase transition at $T = T_c$ takes place. This picture also applies to $\mathcal{N} = 4$ SYM theory with $T_c = 0$, as described in the main text. In $\mathcal{N} = 4$ SYM theory, the top (bottom) panel applies when $M_q > 0$ ($M_q = 0$).

The universal character of the meson dissociation transition was emphasized in Refs. [605, 608], which we will follow in our presentation. Specific examples were originally seen in [92, 560, 534], and aspects of these transitions in the D3/D7 system were studied independently in [37, 38, 351, 514]. Similar holographic transitions appeared in a slightly different framework in [30, 669, 367, 58]. The D3/D7 system at nonzero temperature has been studied upon including the backreaction of the D7-branes in Ref. [161].

9.3.2 Thermodynamics of D7-branes

In this section we shall show that the phase transition between Minkowski and black hole embeddings is a discontinuous, first order phase transition. The reader willing to accept this without proof can safely skip to Section 9.3.3. Since we are working in the canonical ensemble (i.e. at fixed temperature) we must compute the free energy density of the system per unit gauge theory three-volume, F, and determine the configuration that minimizes it. In the gauge theory we know that this takes the form

https://doi.org/10.1017/9781009403504.009 Published online by Cambridge University Press

$$F = F_{\mathcal{N}=4} + F_{\text{flavor}}\,, \tag{9.19}$$

where the first term is the $\mathcal{O}(N_c^2)$ free energy of the $\mathcal{N} = 4$ SYM theory in the absence of quarks, and the second term is the $\mathcal{O}(N_c N_f)$ contribution due to the presence of quarks in the fundamental representation. Since the SYM theory without quarks is conformal, dimensional analysis completely fixes the first factor to be of the form $F_{\mathcal{N}=4} = C(\lambda)T^4$, where C is a possibly coupling-dependent coefficient of order N_c^2. In contrast, in the presence of quarks of mass M_{q} there is a dimensionless ratio T/M_{q} on which the flavor contribution can depend non-trivially. Our purpose is to determine this contribution to leading order in the large-N_c, strong coupling limit.

Our tool is of course the dual description of the $\mathcal{N} = 4$ SYM theory with flavor as a system of N_f D7-brane probes in the gravitational background of N_c black D3-branes. As usual in finite-temperature physics, the free energy of the system may be computed through the identification

$$\beta F = S_{\text{E}}\,, \tag{9.20}$$

where $\beta = 1/T$ and S_{E} is the Euclidean action of the system. In our case this takes the form

$$S_{\text{E}} = S_{\text{sugra}} + S_{\text{D7}}\,. \tag{9.21}$$

The first term is the contribution from the black hole gravitational background sourced by the D3-branes, and is computed by evaluating the Euclideanized supergravity action on this background. The second term is the contribution from the D7-branes, and is computed by evaluating the Euclidean version of the DBI action (4.18) on a particular D7-brane configuration. The decomposition (9.21) is the dual version of that in (9.19). The supergravity action scales as $1/g_s^2 \sim N_c^2$, and thus yields the free energy of the $\mathcal{N} = 4$ SYM theory in the absence of quarks, i.e. we identify

$$S_{\text{sugra}} = \beta F_{\mathcal{N}=4}\,. \tag{9.22}$$

Similarly, the D7-brane action scales as $N_f/g_s \sim N_c N_f$, and represents the flavor contribution to the free energy:

$$S_{\text{D7}} = \beta F_{\text{D7}} = \beta F_{\text{flavor}}\,. \tag{9.23}$$

We therefore conclude that we must first find the solutions of the equations of motion of the D7-branes for any given values of T and M_{q}, then evaluate their Euclidean actions, and finally use the identification above to compare their free energies and determine the thermodynamically preferred configuration.

As explained above, in our case solving the D7-brane equations of motion just means finding the function $U(u)$, which is determined by the condition that the

https://doi.org/10.1017/9781009403504.009 Published online by Cambridge University Press

D7-brane action be extremized. This leads to an ordinary, second order, nonlinear differential equation for $U(u)$. Its precise form can be found in e.g. Ref. [608], but is not very illuminating. However, it is easy to see that it implies the asymptotic, large-u behavior

$$U(u) = \frac{m\, r_0}{\sqrt{2}} + \frac{c\, r_0^3}{2\sqrt{2}\, u^2} + \cdots , \tag{9.24}$$

where m and c are constants. The factors of r_0 have been introduced to make these constants dimensionless, whereas the numerical factors have been chosen to facilitate comparison with the literature. As usual (and, in particular, as in Section 5.1.5), the leading and subleading terms correspond to the non-normalizable and to the normalizable modes, respectively. Their coefficients are therefore proportional to the source and the expectation values of the corresponding dual operator in the gauge theory. In this case, the position of the brane $U(u)$ is dual to the quark mass operator $\mathcal{O}_m \sim \bar{\psi}\psi$, so m and c are proportional to the quark mass and the quark condensate, respectively. The precise form of $\mathcal{O}_m$ can be found in Ref. [539], where it is shown that the exact relation between m, c and $M_{\rm q}$, $\langle \mathcal{O}_m \rangle$ is

$$M_{\rm q} = \frac{r_0 m}{2^{3/2}\pi\, \ell_s^2} = \frac{1}{2\sqrt{2}}\sqrt{\lambda}\, T\, m\,, \tag{9.25}$$

$$\langle \mathcal{O}_m \rangle = -2^{3/2}\pi^3 \ell_s^2 N_f T_{\rm D7} r_0^3\, c = -\frac{1}{8\sqrt{2}}\sqrt{\lambda}\, N_f\, N_c\, T^3\, c\,. \tag{9.26}$$

In particular, we recover the fact that the asymptotic value

$$L = \lim_{u\to\infty} U(u) = \frac{m r_0}{\sqrt{2}} \tag{9.27}$$

is related to the quark mass through Eq. (9.2), as anticipated in previous sections.

It is interesting to note that the dimensionless mass m is given by the simple ratio

$$m = \frac{\bar{M}}{T}\,, \tag{9.28}$$

where

$$\bar{M} = \frac{2\sqrt{2} M_{\rm q}}{\sqrt{\lambda}} = \frac{M_{\rm mes}}{2\pi} \tag{9.29}$$

is (up to a constant) precisely the meson gap at zero temperature, given in Eq. (9.15). As mentioned in Section 9.2.1, and as we will elaborate upon in Section 9.4.3, $\mathcal{O}_m$ must be thought of as the analogue of a heavy or light quark bilinear operator in QCD depending on whether the ratio $M_{\rm mes}/T \sim m$ is large or small, respectively.

The constants m and c can be understood as the two integration constants that completely determine a solution of the second order differential equation obeyed

https://doi.org/10.1017/9781009403504.009 Published online by Cambridge University Press

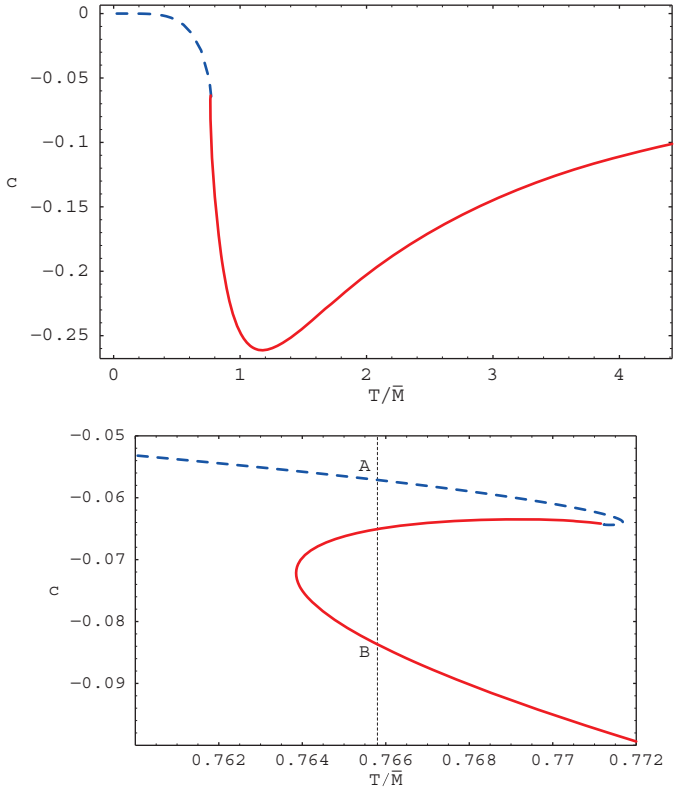

Figure 9.9 Quark condensate c versus $T/\bar{M} = 1/m$. The blue dashed (red continuous) curves correspond to the Minkowski (black hole) embeddings. The dotted vertical line indicates the precise temperature of the phase transition. The point where the two branches meet corresponds to the critical embedding. Figures taken from Refs. [605, 608].

by $U(u)$. Mathematically, these two constants are independent, but the physical requirement that the solution be regular in the interior relates them to one another. The equation for $U(u)$ can be solved numerically (see, e.g. Ref. [608]), and the resulting possible values of c for each value of m are plotted in Fig. 9.9. We see from the "large scale" plot above that c is a single-valued function of m for most values of the latter. However, the zoom-in plot below shows that, in a small region around $1/m = T/\bar{M} \simeq 0.766$, three values of c are possible for a given value of m; a pictorial representation of a situation of this type is shown in Fig. 9.10. This multi-valuedness is related to the existence of the phase transition which, as we will see, proceeds between points A and B through a discontinuous jump in the quark condensate and other physical quantities. The point in Fig. 9.9 where the Minkowski and the black hole branches meet corresponds to the critical embedding.

https://doi.org/10.1017/9781009403504.009 Published online by Cambridge University Press

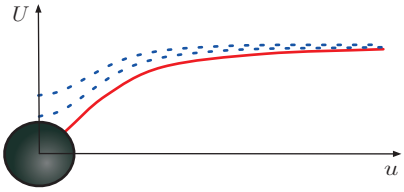

Figure 9.10 Some representative D7-brane embeddings from the region in which c is multi-valued. The three profiles correspond to the same value of m but differ in their value of c. Two of them, represented by blue, dashed curves, are of Minkowski type. The third one, represented by a red, continuous curve, is a black hole embedding.

Having determined the regular D7-brane configurations, one must now compute their free energies and compare them in order to determine which one is preferred in the multivalued region. The result is shown in Fig. 9.11(top), where the normalization constant is given by [605, 608]

$$\mathcal{N} = \frac{2\pi^2 N_f T_{\rm D7} r_0^4}{4T} = \frac{\lambda N_f N_c}{64} T^3 \,. \tag{9.30}$$

The plot on the right shows the classic "swallow tail" form, typically associated with a first order phase transition. As anticipated, Minkowski embeddings have the lowest free energy for temperatures $T < T_{\rm diss}$, whereas the free energy is minimized by black hole embeddings for $T > T_{\rm diss}$, with $T_{\rm diss} \simeq 0.77\bar{M}$ (i.e. $m \simeq 1.3$). At $T = T_{\rm diss}$ the Minkowski and the black hole branches meet and the thermodynamically preferred embedding changes from one type to the other. The first order nature of the phase transition follows from the fact that several physical quantities jump discontinuously across the transition. An example is provided by the quark condensate which, as illustrated in Fig. 9.9, makes a finite jump between the points labelled A and B. Similar discontinuities also appear in other physical quantities, like the entropy and energy density. These are easily obtained from the free energy through the usual thermodynamic relations

$$S = -\frac{\partial F}{\partial T} \,, \qquad E = F + TS \,, \tag{9.31}$$

and the results are shown in Fig. 9.11. From the plots of the energy density one can immediately read off the qualitative behavior of the specific heat $c_V = \partial E/\partial T$. In particular, note that this slope must become negative as the curves approach the critical solution, indicating that the corresponding embeddings are thermodynamically unstable. Examining the fluctuation spectrum of the branes, we will show that a corresponding dynamical instability, manifested by a meson state becoming tachyonic, is present exactly for the same embeddings for which $c_V < 0$. One may

https://doi.org/10.1017/9781009403504.009 Published online by Cambridge University Press

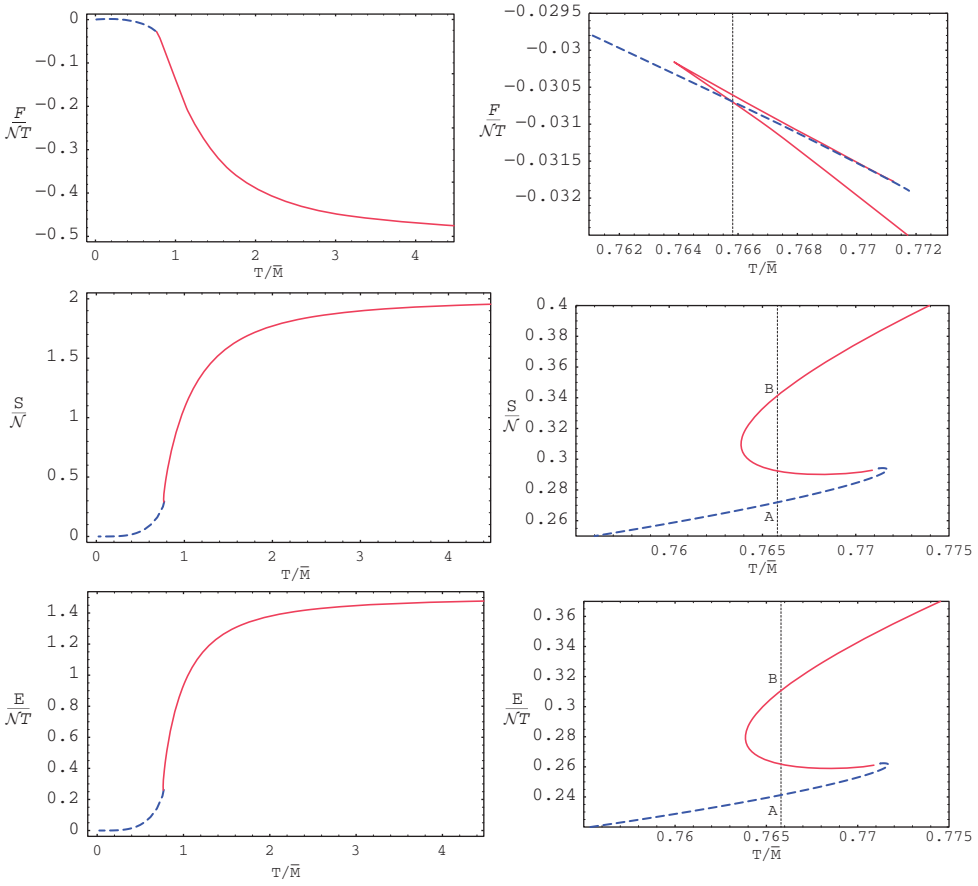

Figure 9.11 Free energy, entropy and energy densities for a D7-brane in a black D3-brane background; note that $\mathcal{N} \propto T^3$. The blue dashed (red continuous) curves correspond to the Minkowski (black hole) embeddings. The dotted vertical line indicates the precise temperature of the phase transition. Figures taken from Refs. [605, 608].

have thought that the phases near the critical point were metastable and thus accessible by "super-cooling" the system, but instead it turns out that over much of the relevant regime such phases are unstable.

We see from (9.30) that $\mathcal{N} \sim \lambda N_c N_f T^3$, which means that the leading contribution of the D7-branes to all the various thermodynamic quantities will be order $\lambda N_c N_f$, in comparison to N_c^2 for the usual bulk gravitational contributions. The $N_c N_f$ dependence, anticipated below Eq. (9.19), follows from large-N_c counting. In contrast, as noted in Refs. [605, 607], the factor of λ represents a strong coupling enhancement over the contribution of a simple free-field estimate for the $N_c N_f$ fundamental degrees of freedom. From the viewpoint of the string description,

https://doi.org/10.1017/9781009403504.009 Published online by Cambridge University Press

this enhancement is easy to understand by reexamining the relative normalization of the two terms in Eq. (9.21) more carefully than we did above. Ignoring only order-one, purely numerical factors, the supergravity action scales as $1/G$, with $G \sim g_s^2 \ell_s^8$ the ten-dimensional Newton's constant, whereas the D7-brane action scales as $N_f T_{\rm D7} \sim N_f / g_s \ell_s^8$. The ratio between the two normalizations is therefore

$$G N_f T_{\rm D7} \sim g_s N_f \sim g^2 N_f \sim \frac{\lambda N_f}{N_c} \,. \tag{9.32}$$

Thus the flavor contribution is suppressed with respect to the leading $\mathcal{O}(N_c^2)$ contribution by $\lambda N_f / N_c$, i.e. it is of order $\lambda N_c N_f$. We will come back to this point in the next section.

As the calculations above were all performed in the limit $N_c, \lambda \to \infty$ (with N_f fixed), it is natural to ask how the detailed results depend on this approximation. Since the phase transition is first order, we expect that its qualitative features will remain unchanged within a finite radius of the $1/N_c$, $1/\lambda$ expansions. Of course, finite-N_c and finite-λ corrections may eventually modify the behavior described above. For example, at large but finite N_c the black hole will emit Hawking radiation and each bit of the probe branes will experience a thermal bath at a temperature determined by the local acceleration. Similarly, finite 't Hooft coupling corrections, which correspond to higher derivative corrections both to the supergravity action and the D-brane action, will become important if the spacetime or the brane curvatures become large. It is certainly clear that both types of corrections will become more and more important as the lower part of a Minkowski brane approaches the horizon, since as this happens the local temperature and the branes (intrinsic) curvature at their tip increase. However, at the phase transition the minimum separation between the branes and the horizon is not parametrically small, and therefore the corrections above can be made arbitrarily small by taking N_c and λ sufficiently large but still finite. This confirms our expectation on general grounds that the qualitative aspects of the phase transition should be robust within a finite radius around the $1/N_c = 0$, $1/\lambda = 0$ point. Of course, these considerations do not tell us whether the dissociation transition is first order or a crossover at $N_c = 3$.

9.3.3 Quarkonium thermodynamics

We have seen above that, in a large class of strongly coupled gauge theories with fundamental matter, this matter undergoes a first order phase transition described on the gravity side by a change in the geometry of the probe D-branes. In this section we will elaborate on thermodynamical aspects of this transition from the gauge theory viewpoint. Once we have learned more about the dynamics of holographic mesons in subsequent sections, in Section 9.4.3 we will return to the gauge

https://doi.org/10.1017/9781009403504.009 Published online by Cambridge University Press

theory viewpoint and discuss possible implications for the dynamics of quarkonium mesons in the QCD plasma.

The temperature scale at which the phase transition takes place is set by the meson gap at zero temperature, $T_{\rm diss} \sim M_{\rm mes}$. As well as giving the mass gap in the meson spectrum, $1/M_{\rm mes}$ is roughly the characteristic size of these bound states [460, 637]. The gluons and other adjoint fields are already in a deconfined phase at $T_{\rm diss}$, so this new transition is not a confinement/deconfinement transition. Rather, the most striking feature of the new phase transition is the change in the meson spectrum, and so we refer to it as a "dissociation" or "melting" transition.

In the low temperature phase, below the transition, stable mesons exist and their spectrum is discrete and gapped. This follows from the same general principles as in the zero-temperature case. The meson spectrum corresponds to the spectrum of normalizable fluctuations of the D7-branes around their fiducial embedding. For Minkowski embeddings the branes close off smoothly outside the black hole horizon and the admissible modes must also satisfy a regularity condition at the tip of the branes. On general grounds, we expect that the regular solution at the tip of the branes evolves precisely into the normalizable solution at the boundary only for a certain set of discrete values of the meson mass. We will study the meson spectrum in detail in Section 9.4.1, and in Section 9.4.2 we will see that mesons acquire finite decay widths at finite N_c or finite coupling. Since the phase under consideration is not a confining phase, we can also introduce deconfined quarks into the system, represented by fundamental strings stretching between the D7-branes and the horizon. At a figurative level, in this phase we might describe quarks in the adjoint plasma as a "suspension". That is, when quarks are added to this phase, they retain their individual identities. More technically, we may just say that quarks are well defined quasiparticles in the Minkowski phase.

In the high temperature phase, at $T > T_{\rm diss}$, no stable mesons exist. Instead, as we will discuss in more detail in Section 9.5, the excitations of the fundamental fields in this phase are characterised by a discrete spectrum of quasinormal modes on the black hole embeddings [469, 638]. The spectral function of some two-point meson correlators in the holographic theory, of which we will see an example in Section 9.5.2, still exhibits some broad peaks in a regime just above $T_{\rm diss}$, which suggests that a few broad bound states persist just above the dissociation phase transition [638, 604]. This is analogous to the lattice approach, where similar spectral functions are examined to verify the presence or absence of bound states. Hence, identifying $T_{\rm diss}$ with the dissociation temperature should be seen as a (small) underestimate of the temperature at which mesons completely cease to exist. An appropriate figurative characterization of the quarks in this high temperature phase would be as a "solution". If one attempts to inject a localized quark charge into the system, it quickly falls through the horizon, i.e. it spreads out

https://doi.org/10.1017/9781009403504.009 Published online by Cambridge University Press

across the entire plasma and its presence is reduced to diffuse disturbances of the supergravity and worldvolume fields, which are soon damped out [469, 638]. Technically speaking, we may just state that quarks are not well-defined quasiparticles in the black hole phase.

The physics above is potentially interesting in connection with QCD since, as we reviewed in Sections 2.4 and 3.3, evidence from several sources indicates that heavy quarkonium mesons remain bound in a range of temperatures above T_c. We will analyze this connection in more detail in Section 9.4.3, once we have learned more about the properties of holographic mesons in subsequent sections. Here we would just like to point out one simple physical parallel. The question of quarkonium bound states surviving in the quark–gluon plasma was first addressed by comparing the size of the bound states to the screening length in the plasma [609]. In the D3/D7 system, the size of the mesons can be inferred, for example, from the structure functions, and the relevant length scale that emerges is $d_{\rm mes} \sim \sqrt{\lambda}/M_{\rm q}$ [460]. This can also be heuristically motivated as follows. As discussed in Section 5.4 (see Eq. (5.86)) at zero temperature the potential between a quark–antiquark pair separated by a distance ℓ is given by

$$V \sim -\frac{\sqrt{\lambda}}{\ell} \,. \tag{9.33}$$

We can then estimate the size $d_{\rm mes}$ of a meson by requiring $E_B \sim |V(d_{\rm mes})|$, where E_B is the binding energy (9.16).[5] This gives

$$d_{\rm mes} \sim \frac{\sqrt{\lambda}}{E_B} \sim \frac{\sqrt{\lambda}}{M_{\rm q}} \sim \frac{1}{M_{\rm mes}} \sim \frac{R^2}{L} \,. \tag{9.34}$$

The last equality follows from Eq. (9.14) and is consistent with expectations based on the UV/IR correspondence [637], since on the gravity side mesons are excitations near $r = L$. Just for comparison, we remind the reader that the weak coupling formula for the size of quarkonium is $d_{\rm weak} \sim 1/(g^2 M_{\rm q})$.

One intuitive way to understand why a meson has a very large size compared to its inverse binding energy or to the inverse quark mass is that, owing to strong coupling effects, the quarks themselves have an effective size of order $d_{\rm mes}$. The effective size of a quark is defined as the largest of the following two scales: (i) its Compton wavelength, or (ii) the distance between a quark–antiquark pair at which their potential energy is large enough to pair-produce additional quarks and antiquarks. In a weakly coupled theory (i) is larger, whereas in a strongly coupled theory (ii) is larger. From Eq. (9.33) we see that this criterion gives an effective quark size of order $\sqrt{\lambda}/M_{\rm q}$ instead of $1/M_{\rm q}$. This heuristic estimate is

[5] Equation (9.16) was derived at zero temperature, but as we will see in Section 9.4.1 it is also parametrically correct at nonzero temperature.

https://doi.org/10.1017/9781009403504.009 Published online by Cambridge University Press

supported by an explicit calculation of the size of the gluon cloud that dresses a quark [465]. These authors computed the expectation value $\langle \mathrm{Tr} F^2(x) \rangle$ sourced by a quark of mass $M_{\rm q}$ and found that the characteristic size of the region in which this expectation value is nonzero is precisely $\sqrt{\lambda}/M_{\rm q}$.

As reviewed in Section 5.4.2, holographic studies of Wilson lines at nonzero temperature [712, 190] reveal that the relevant screening length of the SYM plasma is of order $L_s \sim 1/T$ – see Eq. (8.182). The argument that the mesons should dissociate when the screening length is shorter than the size of these bound states then yields $T_{\rm diss} \sim M_{\rm q}/\sqrt{\lambda} \sim M_{\rm mes}$, in agreement with the results of the detailed calculations explained in previous sections. We thus see that the same physical reasoning which, as we saw in Sections 2.4 and 3.3, has been used in QCD to estimate the dissociation temperature of, e.g., the J/ψ meson can also be used to understand the dissociation of mesons in the $\mathcal{N} = 4$ SYM theory. This may still seem counterintuitive in view of the fact that the binding energy of these mesons is much larger that $T_{\rm diss}$. In other words, one might have expected that the temperature required to break apart a meson would be of the order of the binding energy, $E_B \sim M_{\rm q}$, instead of being parametrically smaller,

$$T_{\rm diss} \sim M_{\rm mes} \sim E_B/\sqrt{\lambda}\,. \tag{9.35}$$

However, this intuition relies on the expectation that the result of dissociating a meson is a quark–antiquark pair of mass $2M_{\rm q}$. The gravity description makes it clear that this is not the case at strong coupling, since above $T_{\rm diss}$ the branes fall through the horizon. Heuristically, one may say that this means that the "constituent" or "thermal" mass of the quarks becomes effectively zero. However, a more precise statement is simply that in the black hole phase quark-like quasiparticles simply do not exist, and therefore for the purpose of the present discussion it becomes meaningless to attribute a mass to them.

One point worth emphasizing is that there are two distinct processes that are occurring at $T \sim M_{\rm mes}$. If we consider, for example, the entropy density in Fig. 9.11, we see that the phase transition occurs in the midst of a crossover signaled by a rise in S/T^3. We may write the contribution of the fundamental matter to the entropy density as

$$S_{\rm flavor} = \frac{1}{8}\lambda\, N_f\, N_c\, T^3\, H(x)\,, \tag{9.36}$$

where $x = \lambda T^2/M_{\rm q}$ and $H(x)$ is the function shown in the plot of the free energy density in the top panels of Fig. 9.11. H rises from 0 at $x = 0$ to 2 as $x \to \infty$, but the most dramatic part of this rise occurs in the vicinity of $x = 1$. Hence it seems that new degrees of freedom, i.e. the fundamental quarks, are becoming "thermally activated" at $T \sim M_{\rm mes}$. We note that the phase transition produces

https://doi.org/10.1017/9781009403504.009 Published online by Cambridge University Press

a discontinuous jump in which H only increases by about 0.07, i.e. the jump at the phase transition only accounts for about 3.5% of the total entropy increase. Thus the phase transition seems to play a small role in this crossover and produces relatively small changes in the thermal properties of the fundamental matter, such as the energy and entropy densities.

As $M_{\rm mes}$ sets the scale of the mass gap in the meson spectrum, it is tempting to associate the crossover above with the thermal excitation of mesonic degrees of freedom. However, the pre-factor $\lambda\, N_f\, N_c$ in (9.36) indicates that this reasoning is incorrect: if mesons provided the relevant degrees of freedom, we should have $S_{\rm flavor} \propto N_f^2$. Such a contribution can be obtained either by a one-loop calculation of the fluctuation determinant around the classical D7-brane configuration, or by taking into consideration the D7-branes' backreaction to second order in the N_f/N_c expansion as in [278, 382, 339, 161]. One can make an analogy here with the entropy of a confining theory (cf. Section 5.2.2). In the low temperature, confining phase the absence of a black hole horizon implies that the classical-gravity saddle point yields zero entropy, which means that the entropy is zero at order N_c^2. One must look at the fluctuation determinant to see the entropy contributed by the supergravity modes, i.e. by the gauge singlet glueballs, which is of order N_c^0.

We thus see that the factor of $N_f N_c$ in $S_{\rm flavor}$ is naturally interpreted as counting the number of degrees of freedom associated with deconfined quarks, with the factor of λ demonstrating that the contribution of the quarks is enhanced at strong coupling. A complementary interpretation of (9.36) comes from reorganizing the pre-factor as

$$\lambda\, N_f\, N_c = (g^2 N_f)\, N_c^2\,. \tag{9.37}$$

The latter expression suggests that the result corresponds to the first order correction of the adjoint entropy due to quark loops. As explained at the end of Section 5.5.1, we are working in a "not quite" quenched approximation, in that contributions of the D7-branes represent the leading order contribution in an expansion in N_f/N_c, and so quark loops are suppressed but not completely. In view of the discussion below Eq. (9.32), it is clear that the expansion for the classical gravitational backreaction of the D7-branes is controlled by $\lambda N_f/N_c = g^2 N_f$. Hence this expansion corresponds to precisely the expansion in quark loops on the gauge theory side.

We conclude that the strongly coupled theory brings together these two otherwise distinct processes. That is, because the $\mathcal{N} = 4$ SYM theory is strongly coupled at all energy scales, the dissociation of the quarkonium bound states and the thermal activation of the quarks happen at essentially the same temperature. Note that this implies that the phase transition should not be thought of as *exclusively* associated with a discontinuous change in the properties of mesons – despite

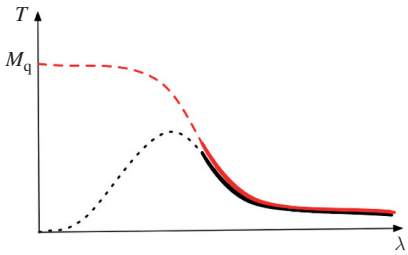

Figure 9.12 A qualitative representation of the simplest possibility interpolating between the weak and the strong coupling regimes in $\mathcal{N} = 4$ SYM theory. The solid and the dotted black curves correspond to $T = T_{\rm diss}$. At strong coupling this corresponds to a first order phase transition (solid black curve), whereas at weak coupling it corresponds to a crossover (dotted black curve). The solid and the dashed red curves correspond to $T = T_{\rm activate}$. At strong coupling this takes place immediately after the phase transition, whereas at weak coupling it is widely separated from $T_{\rm diss}$.

the fact that this is the aspect that is more commonly emphasized. The phase transition is also associated with a discontinuous change in the properties of quarks since, as explained above, these exist as well-defined quasiparticles in the Minkowski phase but not in the black hole phase. In fact, as the discussion around Eq. (9.37) makes clear, in the $\mathcal{O}(N_f N_c)$ - approximation considered here the observed discontinuous jump in the thermodynamic functions comes *entirely* from the discontinuous change in the properties of quarks. In this approximation, the discontinuous jump in the thermodynamic functions associated with the discontinuous change in the properties of mesons simply cannot be detected, since it is of order N_f^2 and its determination would require a one-loop calculation. Fortunately, however, the change in the mesons' properties can be inferred, e.g. from the comparison of their spectra above and below $T_{\rm diss}$.

It is instructive to contrast this behavior with that which is expected to occur at weak coupling. In this regime, one expects that the dissociation of the quarkonium mesons may well be just a crossover rather than a (first order) transition. Moreover, since the weakly bound mesons are much larger than $1/M_{\rm mes} \sim 1/(2M_{\rm q})$, their dissociation transition will occur at a $T_{\rm diss}$ that is much lower than $M_{\rm q}$. On the other hand, the quarks would not be thermally activated until the temperature $T_{\rm activate} \sim M_{\rm q}$, above which the number densities of unbound quarks and antiquarks are no longer Boltzmann-suppressed. Presumably, the thermal activation would again correspond to a crossover rather than a phase transition. The key point is that these two temperatures are widely separated at weak coupling. Figure 9.12 is an "artistic" representation of the simplest behavior that would interpolate between strong and weak coupling. One might expect that the dissociation point and the thermal activation are very close for $\lambda \gg 1$. The line of first order phase transitions

https://doi.org/10.1017/9781009403504.009 Published online by Cambridge University Press

must end somewhere and so one might expect that it terminates at a critical point around $\lambda \sim 1$. Below this point, both processes would only represent crossovers and their respective temperatures would diverge from one another, approaching the weak coupling behavior described above.

We close with a comment about a possible comparison to QCD. Although it would be interesting to look for signs of a crossover or a phase transition associated with quarkonium dissociation, for example in lattice QCD, the above discussion makes it clear that much caution must be exercised in trying to compare with the holographic results described here. The differences can be traced back to the fact that, unlike the holographic theory considered here, QCD is not strongly coupled at the scale set by the mass of the heavy quark or of the corresponding heavy quarkonium meson. For this reason, in QCD the binding energy of a quarkonium meson is $E_B \ll M_{\rm mes} \lesssim 2M_{\rm q}$ and, since one expects that $T_{\rm diss} \sim E_B$, this implies that at the dissociation temperature the quarkonium contribution to (say) the total entropy density would be Boltzmann suppressed, i.e. it would be of order $S_{\rm flavor} \sim N_f^2 \exp(-M_{\rm mes}/T_{\rm diss}) \ll 1$. In contrast, in the holographic set-up there is no exponential suppression because $T_{\rm diss} \sim M_{\rm mes}$. Note also that the quarkonium contribution should scale as N_f^2, and therefore the exponential suppression is a further suppression on top of the already small one-loop contribution discussed in the paragraph above Eq. (9.37). That is, there are two sources of suppression relative to the leading $\mathcal{O}(N_f N_c)$ - contribution in the holographic theory. Although N_f/N_c is not small in QCD, the Boltzmann suppression is substantial and will likely make the thermodynamic effects of any quarkonium dissociation transition quite a challenge to identify.

9.4 Quarkonium mesons in motion and in decay

In previous sections, we examined the thermodynamics of the phase transition between Minkowski and black hole embeddings, and we argued that from the gauge theory viewpoint it corresponds to a meson-dissociation transition. In particular, we argued that quarkonium bound states exist on Minkowski embeddings, i.e. at $T < T_{\rm diss}$, that they are absolutely stable in the large-N_c, strong coupling limit, and that their spectrum is discrete and gapped. We will begin Section 9.4.1 by studying this spectrum quantitatively, which will allow us to understand how the meson spectrum is modified with respect to that at zero temperature, described in Section 9.2.2. The spectrum on black hole embeddings will be considered in Section 9.5.

After describing the spectrum of quarkonium mesons at rest, we will determine their dispersion relations. This will allow us to study mesons in motion with respect to the plasma and, in particular, to determine how the dissociation temperature

https://doi.org/10.1017/9781009403504.009 Published online by Cambridge University Press

depends on the meson velocity. As discussed in Section 2.4, one of the hallmarks of a quark–gluon plasma is the screening of colored objects. Heavy quarkonia provide an important probe of this effect since the existence (or absence) of quark–antiquark bound states and their properties are sensitive to the screening properties of the medium in which they are embedded. In Section 8.7 we studied this issue via computing the potential between an external quark–antiquark pair, at rest in the plasma or moving through it with velocity v. In particular, we found that the dissociation temperature scales with v as

$$T_{\rm diss}(v) \simeq T_{\rm diss}(v=0)(1-v^2)^{1/4}\,, \tag{9.38}$$

which could have important implications for the phenomenon of quarkonium suppression in heavy ion collisions. By studying dynamical mesons in a thermal medium, we will be able to reexamine this issue in a more "realistic" context.

We will show in Section 9.4.2 that both finite-N_c and finite-coupling corrections generate nonzero meson decay widths, as one would expect in a thermal medium. We shall find that the dependence of the widths on the meson momentum yields further understanding of how (9.38) arises.

We will close in Section 9.4.3 with a discussion of the potential connections between the properties of quarkonium mesons in motion in a holographic plasma and those of quarkonium mesons in motion in the QCD plasma.

9.4.1 Spectrum and dispersion relations

In order to determine the meson spectrum on Minkowski embeddings, we proceed as in Section 9.2.2. For simplicity we will focus on fluctuations of the position of the branes $U(u)$ with no angular momentum on the S^3, i.e. we write

$$\delta U = \mathcal{U}(u)\, e^{-i\omega t} e^{i\mathbf{q}\cdot\mathbf{x}}\,. \tag{9.39}$$

The main difference between this equation and its zero-temperature counterpart (9.10) is that in the latter case Lorentz invariance implies the usual relation $\omega^2 - q^2 = M^2$ between the energy ω, the spatial three-momentum q, and the mass M of the meson. At nonzero temperature, boost invariance is broken because the plasma defines a preferred frame in which it is at rest and the mesons develop a non-trivial dispersion relation $\omega(q)$. In the string description this is determined by requiring normalizability and regularity of $\mathcal{U}(u)$: For each value of q, these two requirements are mutually compatible only for a discrete set of values $\omega_n(q)$, where different values of n label different excitation levels of the meson. We define the "rest mass" of a meson as its energy $\omega(0)$ at vanishing three-momentum, $q = 0$, in the rest frame of the plasma.

https://doi.org/10.1017/9781009403504.009 Published online by Cambridge University Press

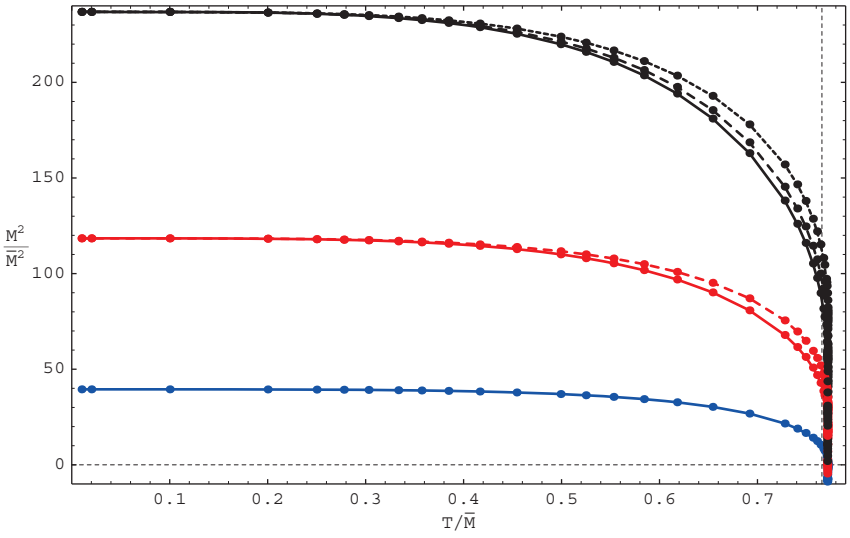

Figure 9.13 Meson mass spectrum $M^2 = \omega^2|_{q=0}$ versus T in units of $\bar{M}$ for Minkowski embeddings in the D3/D7 system. Continuous curves correspond to radially excited mesons with radial quantum number $n = 0, 1, 2$ from bottom to top, respectively. Dashed lines correspond to mesons with angular momentum on the S^3. The dashed vertical line indicates the temperature of the phase transition. Note that modes become tachyonic slightly beyond this temperature. Figure taken from Ref. [608].

Figure 9.13 shows the rest mass of the mesons as a function of temperature and quark mass. Note that in the zero-temperature limit, the spectrum coincides with the zero-temperature spectrum (9.14). In particular, the lightest meson has a mass squared matching Eq. (9.29): $M^2_{\rm mes} = 4\pi^2\bar{M}^2 \simeq 39.5\,\bar{M}^2$.

The meson masses decrease as the temperature increases. Heuristically, this can be understood in geometrical terms from Fig. 9.6, which shows that the thermal quark mass $M_{\rm th}$ decreases as the temperature increases and the tip of the D7-branes gets closer to the black hole horizon. The thermal shift in the meson masses becomes more significant at the phase transition, and slightly beyond this point some modes actually become tachyonic. This happens precisely in the same region in which Minkowski embeddings become thermodynamically unstable because $c_V < 0$. In other words, Minkowski embeddings develop thermodynamic and dynamic instabilities at exactly the same $T/\bar{M}$, just beyond that at which the first order dissociation transition occurs.

We now turn to quarkonium mesons moving through the plasma, that is to modes with $q \neq 0$. The dispersion relation for scalar mesons was first computed in Ref. [608] and then revisited in Ref. [336]. The dispersion relation for (transverse) vector mesons appeared in Ref. [255]. An exhaustive discussion of the dispersion

https://doi.org/10.1017/9781009403504.009 Published online by Cambridge University Press

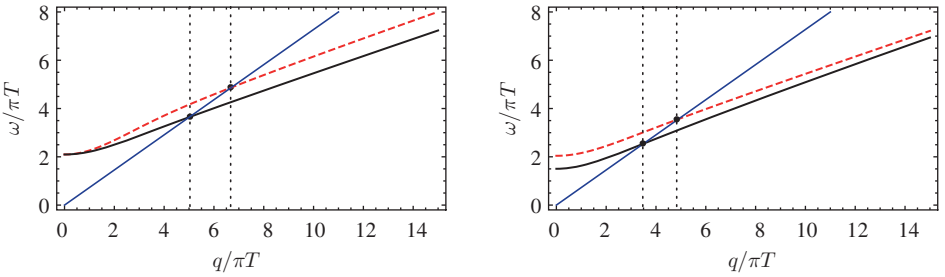

Figure 9.14 Left: dispersion relation for the transverse (black, continuous curve) and longitudinal (red, dashed curve) $n = 0$ modes of a heavy vector meson with $v_{\rm lim} = 0.35$ in the $\mathcal{N} = 4$ SYM plasma. The dual D7-brane has $m = 1.3$, corresponding to a temperature just below $T_{\rm diss}$. Right: analogous curves for a scalar (black, continuous curve) and pseudoscalar (red, dashed curve) meson. In both plots the blue, continuous straight lines correspond to $\omega = vq$ for some v such that $v_{\rm lim} < v \leq 1$. The black, dotted, vertical lines mark the crossing points between the meson dispersion relations and the blue lines. Figure taken from Ref. [256].

relations for all these cases can be found in Ref. [256]. The result for the lowest-lying ($n = 0$) vector, scalar and pseudoscalar quarkonia is shown in Fig. 9.14. Figure 9.15 shows the group velocity $v_g = d\omega/dq$ for the $n = 0$ scalar mesons at three different temperatures.

An important feature of these plots is their behavior at large momentum. In this regime we find that ω grows linearly with q. Naively, one might expect that the constant of proportionality should be one. However, one finds instead that

$$\omega = v_{\rm lim}\, q\ , \tag{9.40}$$

where $v_{\rm lim} < 1$ and where $v_{\rm lim}$ depends on $m = \bar{M}/T$ but at a given temperature is the same for all quarkonium modes. In the particular case of $m = 1.3$, illustrated in Fig. 9.14, one has $v_{\rm lim} \simeq 0.35$. In other words, there is a subluminal limiting velocity for quarkonium mesons moving through the plasma. And, as illustrated in Fig. 9.15, one finds that the limiting velocity decreases with increasing temperature. Figure 9.15 also illustrates another generic feature of the dispersion relations, namely that the maximal group velocity is attained at some $q_m < \infty$ and as q is increased further the group velocity approaches $v_{\rm lim}$ from above. Since v_g at q_m is not much greater than $v_{\rm lim}$, we will not always distinguish between these two velocities. We will come back to the physical interpretation of q_m at the end of this section.

The existence of a subluminal limiting velocity, which was discovered in [608] and subsequently elaborated upon in [336], is easily understood from the perspective of the dual gravity description [608, 336]. Recall that mesonic states have wave

https://doi.org/10.1017/9781009403504.009 Published online by Cambridge University Press

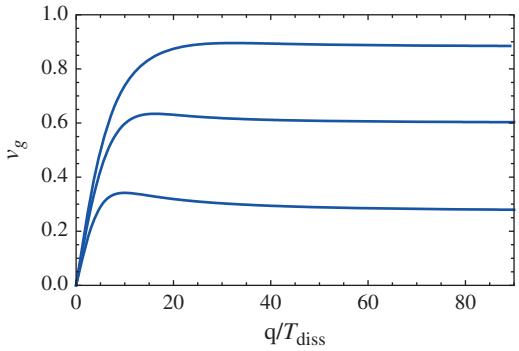

Figure 9.15 Group velocities v_g for $n = 0$ scalar meson modes with $T/T_{\rm diss} \approx 0.65, 0.92$ and 1 from top to bottom. We see that the group velocities approach a limiting value $v_{\rm lim}$ at large q with $v_{\rm lim} < 1$ and with $v_{\rm lim}$ decreasing with increasing temperature. ($v_{\rm lim}$ would approach zero if we included the unstable Minkowski embeddings with $T > T_{\rm diss}$.) The group velocity approaches its large-q value $v_{\rm lim}$ from above, i.e. v_g reaches a maximum before settling into the limiting velocity $v_{\rm lim}$. The maximum exists also for the top curve even though it is less clearly visible. We will refer to the momentum at which v_g reaches the maximum as q_m. Clearly q_m decreases with temperature. Figure taken from Ref. [336].

functions supported on the D7-branes. Since highly energetic mesons are strongly attracted by the gravitational pull of the black hole, their wave function is very concentrated at the bottom of the branes (see Fig. 9.6). Consequently, their velocity is limited by the local speed of light at that point. As seen by an observer at the boundary, this limiting velocity is

$$v_{\rm lim} = \sqrt{-g_{tt}/g_{xx}}\Big|_{\rm tip} \,, \tag{9.41}$$

where g is the induced metric on the D7-branes. Because of the black hole redshift, $v_{\rm lim}$ is lower than the speed of light at infinity (i.e. at the boundary), which is normalized to unity. Note that, as the temperature increases, the bottom of the brane gets closer to the horizon and the redshift becomes larger, thus further reducing $v_{\rm lim}$; this explains the temperature dependence in Fig. 9.15. In the gauge theory, the above translates into the statement that $v_{\rm lim}$ is lower than the speed of light in the vacuum. The reason for this interpretation is that the absence of a medium in the gauge theory corresponds to the absence of a black hole on the gravity side, in which case $v_{\rm lim} = 1$ everywhere. Eq. (9.41) yields $v_{\rm lim} \simeq 0.35$ at $m = 1.3$, in agreement with the numerical results displayed in Fig. 9.14.

It is also instructive to plot $v_{\rm lim}$ as a function of $T/T_{\rm diss}$, as done in Fig. 9.16. Although this curve was derived as a limiting meson velocity at a given temperature, it can also be read (by asking where it cuts horizontal lines rather than vertical

https://doi.org/10.1017/9781009403504.009 Published online by Cambridge University Press

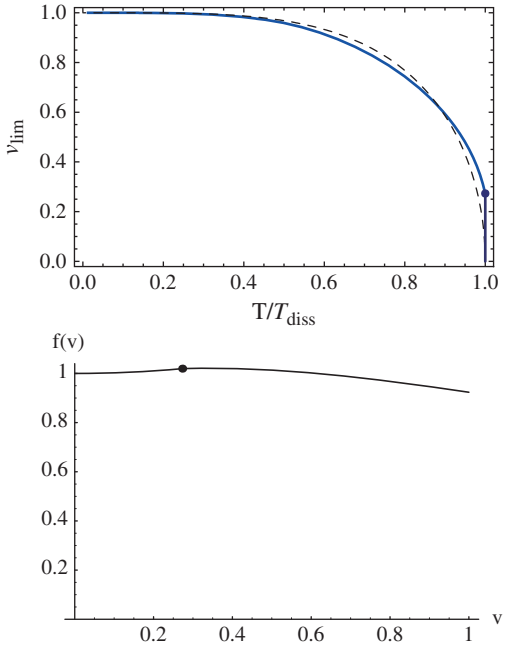

Figure 9.16 Top panel: the solid blue curve is the limiting velocity $v_{\rm lim}$ as a function of $T/T_{\rm diss}$, where $T_{\rm diss}$ is the temperature of the dissociation transition at zero velocity. The dissociation transition occurs at the dot, where $v_{\rm lim} = 0.27$. The dashed black curve is the approximation obtained by setting $f(v) = 1$ in Eq. (9.42). Bottom panel: $f(v)$, the ratio of the solid and dashed curves in the left panel at a given v. We see that $f(v)$ is within a few percent of 1 at all velocities. Figure taken from Ref. [336].

ones) as giving $T_{\rm diss}(v)$, the temperature below which mesons with a given velocity v are found and above which no mesons with that velocity exist. In order to compare this result for $T_{\rm diss}$ at all velocities to (9.38), one can parametrize the curve in Fig. 9.16 as

$$T_{\rm diss}(v) = f(v)(1 - v^2)^{1/4}\, T_{\rm diss}(0)\,. \tag{9.42}$$

In the upper panel of Fig. 9.16, the dashed line is obtained by setting $f(v) = 1$, which is of course just (9.38). In the lower panel, $f(v)$ is shown to be close to 1 for all velocities, varying between 1.021 at its maximum and 0.924 at $v = 1$. Recall that the scaling (9.38) was first obtained via the analysis of the potential between a moving test quark and antiquark, as described in Section 8.7. The weakness of the dependence of $f(v)$ on v is a measure of the robustness with which that simple scaling describes the velocity dependence of the dissociation temperature for quarkonium mesons in a fully dynamical calculation. In other words, to a good

https://doi.org/10.1017/9781009403504.009 Published online by Cambridge University Press

approximation $v_{\rm lim}(T)$ can be determined by setting $v = v_{\rm lim}$ on the right-hand side of (9.38), yielding

$$v_{\rm lim}(T) \simeq \sqrt{1 - \left(\frac{T}{T_{\rm diss}(v=0)}\right)^4}\,. \tag{9.43}$$

Thus we reach a rather satisfactory picture that the subluminal limiting velocity (9.40) is in fact a manifestation in the physics of dynamical mesons of the velocity-enhanced screening of Section 8.7. However, in the case of the low-spin mesons whose dynamics we are considering in this section, there is an important addition to our earlier picture. Although the quarkonium mesons have a limiting velocity, they can nevertheless manage to remain bound at arbitrarily large momenta thanks to their modified dispersion relations. The latter allow the group velocity to remain less than $v_{\rm lim}$, and consequently $T_{\rm diss}(v)$ as given in (9.38) to remain higher than T, all the way out to arbitrarily large momenta. In other words, there exist meson bound states of arbitrarily large spatial momentum, but no matter how large the momentum the group velocity never exceeds $v_{\rm lim}$. In this sense, low-spin mesons realize the first of two simple possibilities by which mesons may avoid exceeding $v_{\rm lim}$. A second possibility, more closely related to the analysis of Section 8.7, is that meson states with momentum larger than a certain value simply cease to exist. This possibility is realized in the case of high-spin mesons. Provided $J \gg 1$, these mesons can be reliably described as long, semi-classical strings whose ends are attached to the bottom of the D7-branes. The fact that the endpoints do not fall on top of one another is of course due to the fact that they are rotating around one another in such a way that the total angular momentum of the string is J. These type of mesons were first studied [559] at zero temperature, and subsequently considered at nonzero temperature in Ref. [674]. These authors also studied the possibility that, at the same time that the endpoints of the string rotate around one another in a given plane, they also move with a certain velocity in the direction orthogonal to that plane. The result of the analysis was that, for a fixed spin J, string solutions exist only up to a maximum velocity $v_{\rm lim} < 1$.

As we saw in Fig. 9.15, the group velocity of quarkonium mesons reaches a *maximum* at some value of the momentum $q = q_m$ before approaching the limiting value $v_{\rm lim}$. There is a simple intuitive explanation for the location of q_m: it can be checked numerically that q_m is always close to the "limiting momentum" $q_{\rm lim}$ that would follow from (9.38) if one assumes the *standard* dispersion relation for the meson. Thus, q_m can be thought of as a characteristic momentum scale where the velocity-enhanced screening effect starts to be important. For the curves in Fig. 9.15, to the left of the maximum one finds approximately standard dispersion relations with a thermally corrected meson mass. To the right of the maximum,

https://doi.org/10.1017/9781009403504.009 Published online by Cambridge University Press

the dispersion relations approach the limiting behavior (9.40), with v_g approaching $v_{\rm lim}$, as a consequence of the enhanced screening.

9.4.2 Decay widths

We saw above that at $T < T_{\rm diss}$ (Minkowski embeddings) there is a discrete and gapped spectrum of absolutely stable quarkonium mesons, i.e. the mesons have zero width. The reason is that in this phase the D-branes do not touch the black hole horizon. Since the mesons' wave functions are supported on the branes, this means that the mesons cannot fall into the black hole. In the gauge theory this translates into the statement that the mesons cannot disappear into the plasma, which implies that the meson widths are strictly zero in the limit $N_c, \lambda \to \infty$. This conclusion only depends on the topology of the Minkowski embedding. In particular, it applies even when higher order perturbative corrections in α' are included, which implies that the widths of mesons should remain zero to all orders in the perturbative $1/\sqrt{\lambda}$ expansion. In contrast, in the black hole phase the D-branes fall into the black hole and a meson has a nonzero probability of disappearing through the horizon, that is, into the plasma. As a consequence, we expect the mesons to develop thermal widths in the black hole phase, even in the limit $N_c, \lambda \to \infty$. In fact, as we will see in Section 9.5, the widths are generically comparable to the energies of the mesons, and hence the mesons can no longer be interpreted as quasiparticles.

We thus encounter a somewhat unusual situation: the quarkonium mesons are absolutely stable for $T < T_{\rm diss}$, but completely disappear for $T > T_{\rm diss}$. The former is counterintuitive because, on general grounds, we expect that any bound states should always have a nonzero width when immersed in a medium with $T > 0$. In the case of these mesons, we expect that they can decay and acquire a width through the following channels:

(1) decay to gauge singlets such as glueballs, lighter mesons, etc;
(2) break up by high energy gluons (right-hand diagram in Fig. 9.17);
(3) break up by thermal medium quarks (left-hand diagram in Fig. 9.17).

Process (1) is suppressed by $1/N_c^2$ (glueballs) or $1/N_c$ (mesons), while (2) and (3) are unsuppressed in the large-N_c limit. Since (1) is also present in the vacuum, we will focus on (2) and (3), which are medium effects. They are shown schematically in Fig. 9.17.

The width due to (2) is proportional to a Boltzmann factor $e^{-\beta E_B}$ for creating a gluon that is energetic enough to break up the bound state, while that due to (3) is proportional to a Boltzmann factor $e^{-\beta M_{\rm th}}$ for creating a thermal quark, where $M_{\rm th}$ is the thermal mass of the quark – see Fig. 9.6. Given Eq. (9.35) and

https://doi.org/10.1017/9781009403504.009 Published online by Cambridge University Press

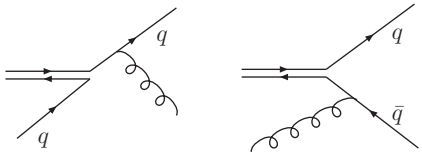

Figure 9.17 Sketches taken from Ref. [347] showing the relevant thermal processes contributing to the meson width. q ($\bar{q}$) denotes a quark (antiquark). The left-hand diagram corresponds to the breakup of a meson by a quark from the thermal medium, while the right-hand diagram corresponds to break up of a meson by an energetic gluon. For large λ the first process is dominant, coming from the single instanton sector.

the fact that in the Minkowski phase $T < T_{\rm diss}$, both Boltzmann factors are suppressed by $e^{-\sqrt{\lambda}} \sim e^{-R^2/\alpha'}$, so we recover the result that these mesons are stable in the infinite-λ limit. In particular, there is no width at any perturbative order in the $1/\sqrt{\lambda}$ expansion, consistent with the conclusion from the string theory side. Furthermore, since the binding energy is $E_B \approx 2M_{\rm th}$, in the regime where λ is large (but not infinite), the width from process (3) will dominate over that from process (2).

We now describe the result from the string theory calculation of the meson widths in Ref. [347]. As discussed above, the width is nonperturbative in $1/\sqrt{\lambda} \sim \alpha'/R^2$, and thus should correspond to some instanton effect on the string worldsheet. The basic idea is very simple: even though in a Minkowski embedding the brane is separated from the black hole horizon and classically a meson living on the brane cannot fall into the black hole, quantum mechanically (from the viewpoint of the string worldsheet) it has a nonzero probability of tunneling into the black hole and the meson therefore develops a width. At leading order, the instanton describing this tunneling process is given by a (Euclidean) string worldsheet stretching between the tip of the D7-brane to the black hole horizon (see Fig. 9.6) and winding around the Euclidean time direction. Heuristically, such a worldsheet creates a small tunnel between the brane and the black hole through which mesons can fall into the black hole. The instanton action is $\beta M_{\rm th}$, as can be read off immediately from the geometric picture just described, and its exponential gives rise to the Boltzmann factor expected from process (3). From the gauge theory perspective, such an instanton can be interpreted as creating a thermal quark from the medium, and a meson can disappear into the medium via interaction with it as shown in the left diagram of Fig. 9.17.

The explicit expression for the meson width due to such instantons is somewhat complicated, so we refer the reader to the original literature [347]. Although the width appears to be highly model dependent and is exponentially small in the regime of a large but finite λ under consideration, remarkably its momentum

https://doi.org/10.1017/9781009403504.009 Published online by Cambridge University Press

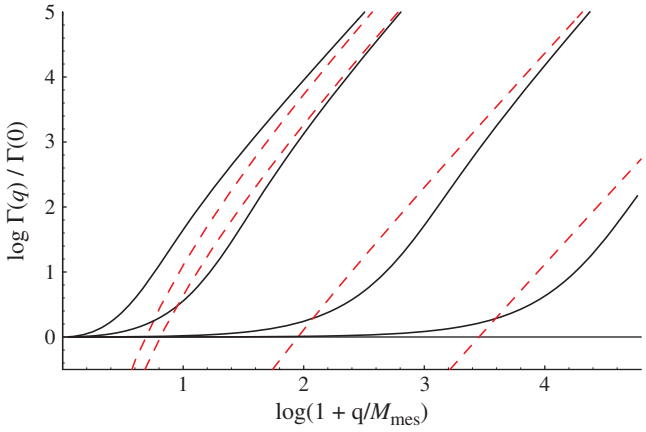

Figure 9.18 The behavior of the width as a function of q for $T/T_{\rm diss} = 0.99,\ 0.71,\ 0.3,\ 0.13$ from left to right. The solid black curves are the full results (9.44); the red dashed curves are the analytic results (9.45) for large momenta. Figure taken from Ref. [347].

dependence has some universal features at large momentum [347]. Specifically, one finds that

$$\frac{\Gamma(q)}{\Gamma(0)} = \frac{|\psi(\text{tip};\vec{q})|^2}{|\psi(\text{tip};\vec{q}=0)|^2}\,, \tag{9.44}$$

where $\Gamma(q)$ denotes the width of a meson with spatial momentum q and $\psi(\text{tip};q)$ its wave function evaluated at the tip of the D7-branes (i.e. where it is closest to the black hole). This result is intuitively obvious because a meson tunnels into the black hole from the tip of the branes. In particular, as discussed in detail in Ref. [336], at large momentum q the wave function becomes localized around the tip of the brane and can be approximated by that of a spherical harmonic oscillator with a potential proportional to q^2z^2, where z is the proper distance from the tip of the branes.[6] It then immediately follows that for large q the width (9.44) scales as q^2. Furthermore for temperatures $T \ll M_{\rm mes}$ and $q \gg M_{\rm mes}^3/T^2$, one finds the closed form expression

$$\frac{\Gamma_n(q)}{\Gamma_n(0)} \approx \frac{2(4\pi)^4}{(n+2)(n+3/2)}\frac{T^4q^2}{M_{\rm mes}^6}\,, \tag{9.45}$$

where n labels different mesonic excitations (see (9.13)).

It is also instructive to plot the full q-dependence of (9.44) obtained numerically, as done in Figure 9.18 for $n = 0$ mesons at various temperatures. Figure 9.18 has the interesting feature that the width is roughly constant for small q, but turns

[6] Note that there are four transverse directions along the D7-brane as we move away from the tip (not including the other $(3+1)$ dimensions parallel to the boundary). Thus this is a four-dimensional harmonic oscillator.

https://doi.org/10.1017/9781009403504.009 Published online by Cambridge University Press

up quadratically around $q/M_{\rm mes} \approx 0.52(T_{\rm diss}/T)^2$. This is roughly the momentum $q_m \sim q_{\rm lim}$ at which the group velocity of a meson achieves its maximum in Fig. 9.15 which, as discussed in Section 9.4.1, can be considered as the characteristic momentum scale where velocity-enhanced screening becomes significant. This dramatic increase of meson widths beyond q_m can also be understood intuitively: when velocity-enhanced screening becomes significant, interaction between the quark and antiquark in a meson becomes further weakened, which makes it easier for a thermal medium quark or gluon to break it apart.

We now briefly comment on the gravity description of process (2) mentioned earlier, i.e. the right-hand diagram in Fig. 9.17. For such a process to happen the gluon should have an energy above the binding energy of the meson. The density of such gluons is thus suppressed by $e^{-2\beta M_{\rm th}}$ and should be described by an instanton and anti-instanton. We expect that contributions from such processes are also controlled by the the value of the meson wave function at the tip of the branes, and thus likely have similar growth with momentum.

Finally, we note that, as T increases, $M_{\rm th}$ decreases and thus the meson width increases quickly with temperature, but remains exponentially suppressed until $T_{\rm diss}$ is reached, after which we are in the black hole phase. As will be discussed in Section 9.5, in this phase quarkonium quasiparticles no longer exist.

9.4.3 Connection with the quark–gluon plasma

Let us now recapitulate the main qualitative features regarding heavy quarkonium mesons in a strongly coupled plasma.

(1) They survive deconfinement.
(2) Their dispersion relations have a subluminal limiting velocity at large momentum. The limiting velocity decreases with increasing temperature and as a result the motion of a meson with large momentum dramatically slows down near $T_{\rm diss}$.
(3) At large momenta, meson widths increase dramatically with momentum.
(4) The limiting velocity is reached and the increase in widths applies when $q \gg q_{\rm lim}$, where $q_{\rm lim}$ is the "limiting" momentum following from (9.38) if one assumes the *standard* dispersion relation.

Properties (1)–(3) are universal in the sense that they apply to the deconfined phase of any gauge theory with a string dual in the large-N_c, strong-coupling limit. The reason for this is that they are simple consequences of general geometric features following from two universal aspects of the gauge/string duality: (i) the fact that the deconfined phase of the gauge theory is described on the gravity side by a black hole geometry [804], and (ii) the fact that a finite number N_f of quark flavors

https://doi.org/10.1017/9781009403504.009 Published online by Cambridge University Press

is described by N_f D-brane probes [517, 513]. Property (4) was established by explicit numerical calculations in specific models. However, given that $q_{\rm lim}$ can be motivated in a model-independent way from (9.38), it is likely to also be universal even though this was not manifest in our discussion above.

We have seen that properties (2) and (3) can be considered direct consequences of velocity-enhanced screening, which as discussed in Section 8.7 can have important implications for quarkonium suppression in heavy ion collisions.

It is interesting that properties (1) and to some degree (2) can be independently motivated in QCD whether or not a string dual of QCD exists. The original argument [609] for (1) is simply that the heavier the quarkonium meson, the smaller its size. And, it is reasonable to expect a meson to remain bound until the screening length in the plasma becomes comparable to the meson size, and for sufficiently heavy quarkonia this happens at $T_{\rm diss} > T_c$. As we have discussed in Sections 2.4 and 3.3, this conclusion is supported by calculations of both the static quark–antiquark potential and of Minkowski space spectral functions in lattice-regularized QCD. The ballpark estimate for the dissociation temperature of heavy mesons suggested by the above studies roughly agrees with that from the D3/D7 system. For example, for the J/ψ meson the former estimate is $T_c \lesssim T_{\rm diss} \lesssim 2T_c$. Allowing for a certain range in the precise value of $150\,{\rm MeV} \lesssim T_c \lesssim 190\,{\rm MeV}$, this translates into $300\,{\rm MeV} \lesssim T_{\rm diss} \lesssim 380\,{\rm MeV}$. In the D3/D7 model, we see from Fig. 9.11 that meson states melt at $T_{\rm diss} \simeq 0.766\bar{M}$. The scale $\bar{M}$ is related to the mass $M_{\rm mes}$ of the lightest meson in the theory at zero temperature through Eq. (9.29). Therefore we have $T_{\rm diss}(M_{\rm mes}) \simeq 0.122 M_{\rm mes}$. For the J/ψ, taking $M_{\rm mes} \simeq 3$ GeV gives $T_{\rm diss}(J/\psi) \simeq 366$ MeV. Although it is gratifying that this comparison leads to qualitative agreement, it must be taken with some caution because meson bound states in the D3/D7 system are deeply bound, i.e. $M_{\rm mes} \ll 2M_{\rm q}$, whereas the binding energy of charmonium states in QCD is a small fraction of the charm mass, i.e. $M_{c\bar{c}} \simeq 2M_c$. An additional difference comes from the fact that in QCD the dissociation of charmonium states is expected to happen sequentially, with excited states (that are larger) dissociating first, whereas in the D3/D7 system all meson states are comparable in size and dissociate at the same temperature. Presumably, in the D3/D7 system this is an artifact of the large-N_c, strong coupling approximation under consideration, and thus corrections away from this limit should make holographic mesons dissociate sequentially too.

There is a simple (but incomplete) argument for property (2) that applies to QCD just as well as to $\mathcal{N} = 4$ SYM theory [583, 674, 281, 336]: a meson moving through the plasma with velocity v experiences a higher energy density, boosted by a factor of γ^2. Since energy density is proportional to T^4, this can be thought of as if the meson sees an effective temperature that is boosted by a factor of $\sqrt{\gamma}$, meaning $T_{\rm eff}(v) = (1 - v^2)^{-1/4} T$. A velocity-dependent dissociation temperature

https://doi.org/10.1017/9781009403504.009 Published online by Cambridge University Press

scaling like (9.38) follows immediately and from this a subluminal limiting velocity (9.43) can be inferred. Although this argument is seductive, it can be seen in several ways that it is incomplete. For example, we would have reached a different $T_{\rm eff}(v)$ had we started by observing that the entropy density s is boosted by a factor of γ and is proportional to T^3. And, furthermore, there really is no single effective temperature seen by the moving quarkonium meson. The earliest analysis of quarkonia moving through a weakly coupled QCD plasma with some velocity v showed that the meson sees a blue-shifted temperature in some directions and a red-shifted temperature in others [296]. Although the simple argument does not work by itself, it does mean that all we need from the calculations done via gauge/string duality is the result that $T_{\rm diss}(v)$ behaves as if it is controlled by the boosted energy density – i.e. we need the full calculation only for the purpose of justifying the use of the particular simple argument that works. This suggests that property (2), and in particular the scaling in Eqs. (9.38) and (9.43), are general enough that they may apply to the quark–gluon plasma of QCD whether or not it has a gravity dual.

As explained towards the end of Section 9.4.1, there are at least two simple ways in which a limiting velocity for quarkonia may be implemented. It may happen that meson states with momentum above a certain $q_{\rm lim}$ simply do not exist, in which case one expects that $v_{\rm lim} = v(q_{\rm lim})$. The second possibility is that the dispersion relation of mesons may become dramatically modified beyond a certain $q_{\rm lim}$ in such a way that, although meson states of arbitrarily high momentum exist, their group velocity never exceeds a certain $v_{\rm lim}$. It is remarkable that both possibilities are realized in gauge theories with a string dual, the former by high-spin mesons and the latter by low-spin mesons. However, note that even in the case of low-spin mesons, $q_{\rm lim}$ remains the important momentum scale beyond which we expect more significant quarkonium suppression for two reasons. First, meson widths increase significantly for $q > q_{\rm lim}$. Therefore, although it is an overstatement to say that these mesons also cease to exist above $q_{\rm lim}$, their existence becomes more and more transient at higher and higher q. Second, owing to the modified dispersion relation mesons with $q > q_{\rm lim}$ slow down and they spend a longer time in the medium, giving the absorptive imaginary part more time to cause dissociation. It will be very interesting to see whether future measurements at RHIC or the LHC will show the suppression of J/ψ or Υ production increasing markedly above some threshold transverse momentum p_T, as we described in Section 8.7.

In practice, our ability to rigorously verify the properties (1)–(4) in QCD is limited due to the lack of tools that are well suited for this purpose. It is therefore reassuring that they hold for all strongly coupled, large-N_c plasmas with a gravity dual, for which the gravity description provides just such a tool.

9.5 Black hole embeddings

We now consider the phase $T > T_{\rm diss}$, which is described by a D7-brane with a black hole embedding. We will give a qualitative argument that in this regime the system *generically* contains no quarkonium quasiparticles. We have emphasized the word "generically" because exceptions arise when certain large ratios of physical scales are introduced "by hand", as we will see later. We will illustrate the absence of quasiparticles in detail by computing a spectral function of two electromagnetic currents in the next section.

9.5.1 Absence of quasiparticles

In the gravity description of physics at $T > T_{\rm diss}$, the meson widths may be seen by studying the quasinormal modes of the D7-brane, analogous to the quasinormal modes of the AdS black brane that we introduced in Section 6.4. The quasinormal modes of the D7-brane are also analogs of the fluctuations we studied in the case of Minkowski embeddings in that a normalizable fall-off is imposed at the boundary. However, the regularity condition at the tip of the branes is replaced by the so-called infalling boundary condition at the horizon. Physically, this is the requirement that energy can flow into the horizon but cannot come out of it (classically). Mathematically, it is easy to see that this boundary condition forces the frequency of the mode to acquire a negative imaginary part, and thus corresponds to a nonzero meson width. The meson in question may then be considered a quasiparticle if and only if this width is much smaller than the real part of the frequency. In the case at hand, the meson widths increase as the area of the induced horizon on the branes increases, and go to zero only when the horizon shrinks to zero size. This is of course to be expected, since it is the presence of the induced horizon that causes the widths to be nonzero in the first place. We are thus led to the suggestion that meson-like quasiparticles will be present in the black hole phase only when the size of the induced horizon on the branes can be made parametrically small. This expectation can be directly verified by explicit calculation of the quasinormal modes on the branes [469, 345, 510, 509], and we will confirm it indirectly below by examining the spectral function of two electromagnetic currents. For the moment, let us just note that this condition is not met in the system under consideration because, as soon as the phase transition at $T = T_{\rm diss}$ takes place, the area of the induced horizon on the brane is an order-one fraction of the area of the background black hole. This can be easily seen from Fig. 9.11 by comparing the entropy density (which is a measure of the horizon area) at the phase transition to the entropy density at asymptotically high temperatures:

$$\frac{s_{\rm transition}}{s_{\rm high\,T}} \approx \frac{0.3}{2} \approx 15\% \,. \tag{9.46}$$

https://doi.org/10.1017/9781009403504.009 Published online by Cambridge University Press

This indicates that there is no *parametric* reason to expect quasiparticles with narrow widths above the transition. We shall confirm by explicit calculation in the next section that there are no quasiparticle excitations in the black hole phase.

9.5.2 Meson spectrum from a spectral function

Here we will illustrate some of the general expectations discussed above by examining the in-medium spectral function of two electromagnetic currents in the black hole phase. We choose this particular correlator because it is the analogue of the correlator that we discussed in Section 3.3 and hence is related to thermal photon production, which we will discuss in the next section. We will see that no narrow peaks exist for stable black hole embeddings, indicating the absence of long-lived quasiparticles. These peaks will appear, however, as we artificially push the system into the unstable region close to the critical embedding (see Fig. 9.7), thus confirming our expectation that quasiparticles should appear as the area of the induced horizon on the branes shrinks to zero size.

$\mathcal{N} = 4$ SYM coupled to N_f flavors of equal-mass quarks is an $SU(N_c)$ gauge theory with a global $U(N_f)$ symmetry. In order to couple this theory to electromagnetism we should gauge a $U(1)_{\rm EM}$ subgroup of $U(N_f)$ by adding a dynamical photon A_μ to the theory; for simplicity we will assume that all quarks have equal electric charge, in which case $U(1)_{\rm EM}$ is the diagonal subgroup of $U(N_f)$. In this extended theory we could then compute correlation functions of the conserved current $J^{\rm EM}_\mu$ that couples to the $U(1)_{\rm EM}$ gauge field. The string dual of this $SU(N_c) \times U(1)_{\rm EM}$ gauge theory is unknown, so we cannot perform this calculation holographically. However, as noted in [239], we can perform it to leading order in the electromagnetic coupling constant e, because at this order correlation functions of electromagnetic currents in the gauged and in the ungauged theories are identical. This is very simple to understand diagramatically, as illustrated for the two-point function in Fig. 9.19. In the ungauged theory only $SU(N_c)$ fields "run" in the loops, represented by the shaded blob. The gauged theory contains additional diagrams in which the photon also runs in the loops, but these necessarily involve more photon vertices and therefore contribute at higher orders in e. Thus one can use the holographic description to compute the "$SU(N_c)$ blob" and obtain the result for the correlator to leading order in e.

Using this observation, the authors of Ref. [239] first did a holographic computation of the spectral density of two R-symmetry currents in $\mathcal{N} = 4$ SYM theory, to which finite-coupling corrections were computed in [428, 429]. The result for the R-charge spectral density is identical, up to an overall constant, with the spectral density of two electromagnetic currents in $\mathcal{N} = 4$ SYM theory coupled to massless quarks. This, and the extension to nonzero quark mass, were obtained in Ref. [604], which we now follow.

https://doi.org/10.1017/9781009403504.009 Published online by Cambridge University Press

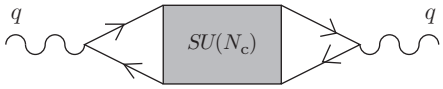

Figure 9.19 Diagrams contributing to the two-point function of electromagnetic currents. The external line corresponds to a photon of momentum q. As explained in the text, to leading order in the electromagnetic coupling constant only $SU(N_c)$ fields "run" in the loops represented by the shaded blob. Figure taken from Ref. [604].

The relevant spectral function is defined as

$$\chi_{\mu\nu}(k) = 2\,\mathrm{Im}\,G^R_{\mu\nu}(k)\,, \tag{9.47}$$

where $k^\mu = (\omega, q)$ is the photon null momentum (i.e. $\omega^2 = q^2$) and

$$G^R_{\mu\nu}(k) = i\int d^{d+1}x\, e^{-ik_\mu x^\mu}\,\Theta(t)\langle[J^{\rm EM}_\mu(x),\, J^{\rm EM}_\nu(0)]\rangle \tag{9.48}$$

is the retarded correlator of two electromagnetic currents. The key point in this calculation is to identify the field in the string description that is dual to the operator of interest here, namely the conserved current $J^{\rm EM}_\mu$. We know from the discussion in Chapter 5 that conserved currents are dual to gauge fields on the string side. Moreover, since $J^{\rm EM}_\mu$ is constructed out of fields in the fundamental representation, we expect its dual field to live on the D7-branes. The natural (and correct) candidate turns out to be the $U(1)$ gauge field associated with the diagonal subgroup of the $U(N_f)$ gauge group living on the worldvolume of the N_f D7-branes. Once this is established, one must just follow the general prescription explained in Chapter 5. The technical details of the calculation can be found in Ref. [604], so here we will describe only the results and their interpretation. In addition, we will concentrate on the trace of the spectral function, $\chi^\mu_{\ \mu}(k) \equiv \eta^{\mu\nu}\chi_{\mu\nu}(k)$, since this is the quantity that determines the thermal photon production by the plasma (see next section).

The trace of the spectral function for stable black hole embeddings is shown in Fig. 9.20 for several values of the quark mass m. Note that this is a function of only one variable, since for an on-shell photon $\omega = q$. The normalisation constant that sets the scale on the vertical axis is $\tilde{\mathcal{N}}_{\rm D7} = N_f N_c T^2/4$. The $N_f N_c$ scaling of the spectral function reflects the number of electrically charged degrees of freedom in the plasma; in the case of two R-symmetry currents, $N_f N_c$ would be replaced by N_c^2 [239]. All curves decay as $\omega^{-1/3}$ for large frequencies. Note that $\chi \sim \omega$ as $\omega \to 0$. This is consistent with the fact that the value at the origin of each of the curves yields the electric conductivity of the plasma at the corresponding quark mass, namely

$$\sigma = \frac{e^2}{4}\lim_{\omega\to 0}\frac{1}{\omega}\eta^{\mu\nu}\chi_{\mu\nu}(\omega = q)\,. \tag{9.49}$$

https://doi.org/10.1017/9781009403504.009 Published online by Cambridge University Press

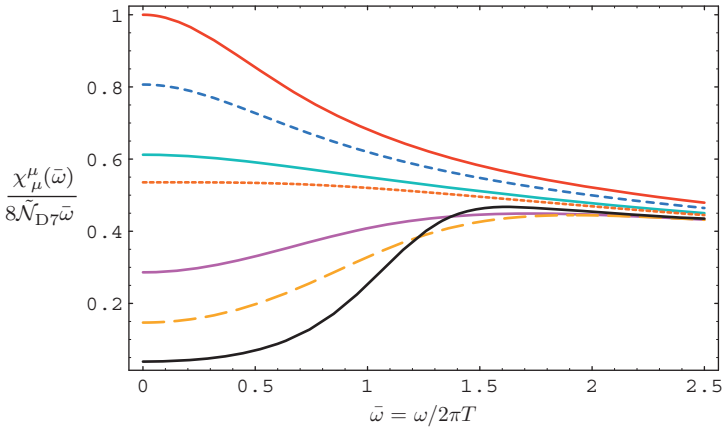

Figure 9.20 Trace of the spectral function as a function of the dimensionless frequency $\bar{\omega} = \omega/2\pi T$ for (from top to bottom on the left-hand side) $m = \{0, 0.6, 0.85, 0.93, 1.15, 1.25, 1.32\}$. The last value corresponds to that at which the phase transition from a black hole to a Minkowski embedding takes place. Recall that $\tilde{\mathcal{N}}_{\rm D7} = N_f N_c T^2/4$. Figure taken from Ref. [604].

This formula is equivalent to the perhaps-more-familiar expression in terms of the zero-frequency limit of the spectral function at vanishing spatial momentum (see Appendix A):

$$\sigma = \frac{e^2}{6} \lim_{\omega\to 0} \frac{1}{\omega} \delta^{ij} \chi_{ij}(\omega, q = 0) = \frac{e^2}{6} \lim_{\omega\to 0} \frac{1}{\omega} \eta^{\mu\nu} \chi_{\mu\nu}(\omega, q = 0)\,, \tag{9.50}$$

where in the last equality we used the fact that $\chi_{00}(\omega \neq 0, q = 0) = 0$, as implied by the Ward identity $k^{\mu}\chi_{\mu\nu}(k) = 0$. To see that the two expressions (9.49) and (9.50) are equivalent, suppose that q points along the 1-direction. Then the Ward identity, together with the symmetry of the spectral function under the exchange of its spacetime indices, imply that $\omega^2\chi_{00} = q^2\chi_{11}$. For null momentum this yields $-\chi_{00} + \chi_{11} = 0$, so we see that Eq. (9.49) reduces to

$$\sigma = \frac{e^2}{4} \lim_{\omega\to 0} \frac{1}{\omega} \Big[\chi_{22}(\omega = q) + \chi_{33}(\omega = q) \Big]. \tag{9.51}$$

The diffusive nature of the hydrodynamic pole of the correlator implies that at low frequency and momentum the spatial part of the spectral function behaves as

$$\chi_{ij}(\omega, q) \sim \frac{\omega^3}{\omega^2 + D^2 q^4}\,, \tag{9.52}$$

where D is the diffusion constant for electric charge. This means that we can replace $q = \omega$ by $q = 0$ in Eq. (9.51), thus arriving at the expression (9.50).

https://doi.org/10.1017/9781009403504.009 Published online by Cambridge University Press

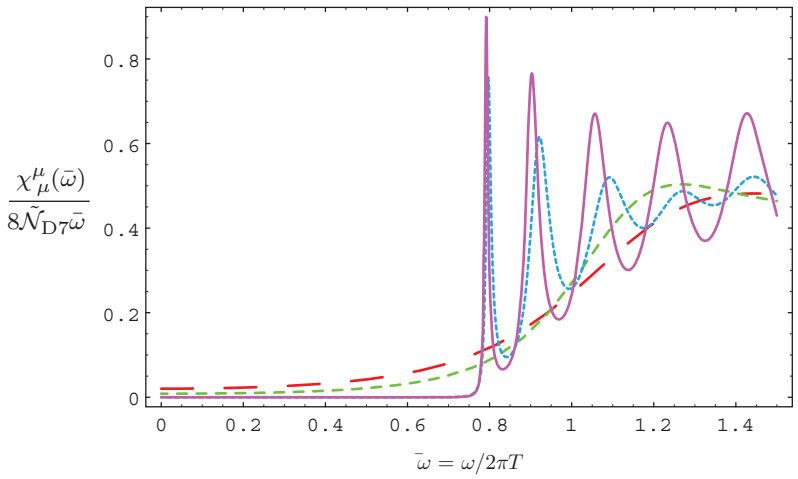

Figure 9.21 Trace of the spectral function as a function of the dimensionless frequency $\bar{\omega} = \omega/2\pi T$ for non-stable black hole embeddings. Curves with higher, narrower peaks correspond to embeddings that are closer to the critical embedding. Figure taken from Ref. [604].

Evaluating (9.50) in the case of massless fundamental matter yields the explicit result [604]

$$\sigma = \frac{1}{4\pi} e^2 N_c N_f T \tag{9.53}$$

that we quoted previously as (6.51). For the case of fundamental matter with mass, the result (9.53) is multiplied by a decreasing function of $m = \bar{M}/T$, defined in (9.28), that becomes very small near the phase transition from a black hole embedding to a Minkowski embedding [604].

For the purpose of our discussion, the most remarkable feature of the spectral functions displayed in Fig. 9.20 is the absence of any kind of high, narrow peaks that may be associated with a quasiparticle excitation in the plasma. This feature is shared by thermal spectral functions of other operators on stable black hole embeddings. We thus confirm our expectation that no quasiparticles exist in this phase. In order to make contact with the physics of the Minkowski phase, in which we do expect the presence of quarkonium quasiparticles, the authors of Ref. [604] computed the spectral function for black hole embeddings beyond the phase transition, i.e. in the region below $T_{\rm diss}$ in which these embeddings are metastable or unstable. The results for the spectral function are shown in Fig. 9.21. The most important feature of these plots is the appearance of well defined peaks in the spectral function, which become higher and narrower, seemingly approaching delta-functions, as the embedding approaches the critical embedding (see Fig. 9.7). Thus the form of the spectral function appears to approach the form we expect for Minkowski

https://doi.org/10.1017/9781009403504.009 Published online by Cambridge University Press

embeddings,[7] namely an infinite sum of delta-functions supported at a discrete set of energies $\omega^2 = q^2$. (However, a precise map between the peaks in Fig. 9.21 and the meson spectrum in a Minkowski embedding is not easy to establish [667].) Each of these delta-functions is associated with a meson mode on the D7-branes with *null* four-momentum. The fact that the momentum is null may seem surprising in view of the fact that, as explained above, the meson spectrum in the Minkowski phase possesses a mass gap, but in fact it follows from the dispersion relation for these mesons displayed in Fig. 9.14. To see this, consider the dispersion relation $\omega(q)$ for a given meson in the Minkowski phase. The fact that there is a mass gap means that $\omega > 0$ at $q = 0$. On the other hand, in the limit of infinite spatial momentum, $q \to \infty$, the dispersion relation takes the form $\omega \simeq v_{\rm lim} q$ with $v_{\rm lim} < 1$. Continuity then implies that there must exist a value of q such that $\omega(q) = q$. This is illustrated in Fig. 9.14 by the fact that the dispersion relations intersect the blue lines. Since in the Minkowski phase the mesons are absolutely stable in the large-N_c, strong coupling limit under consideration, we see that each of them gives rise to a delta-function-like (i.e. zero-width) peak in the spectral function of electromagnetic currents at null momentum. Below we will see some potential implications of this result for heavy ion collisions.

9.6 Two universal predictions

We have just seen that the fact that heavy mesons remain bound in the plasma, and the fact that their limiting velocity is subluminal, imply that the dispersion relation of a heavy meson must cross the lightcone, defined by $\omega = q$, at some energy $\omega = \omega_{\rm peak}$ indicated by the vertical line in Fig. 9.14. In this section we will see that this simple observation leads to two universal consequences. Implications for deep inelastic scattering have been studied in [479] but will not be reviewed here.

9.6.1 A meson peak in the thermal photon spectrum

At the crossing point between the meson dispersion relation and the lightcone, the meson four-momentum is null, that is $\omega^2_{\rm meson} = q^2_{\rm meson}$. If the meson is flavorless and has spin one, then at this point its quantum numbers are the same as those of a photon. Such a meson can then decay into an on-shell photon, as depicted in Fig. 9.22. Note that, in the vacuum, only the decay into a virtual photon would be allowed by kinematics. In the medium, the decay can take place because of the modified dispersion relation of the meson. Also, note that the decay will take place unless the photon–meson coupling vanishes for some reason (e.g. a symmetry). No such reason is known in QCD.

[7] An analogous result was found in [638] for time-like momenta.

https://doi.org/10.1017/9781009403504.009 Published online by Cambridge University Press

Figure 9.22 In-medium vector meson–photon mixing. The imaginary part of this diagram yields the meson decay width into photons. Figure adapted from Ref. [602].

The decay process of Fig. 9.22 contributes a resonance peak, at a position $\omega = \omega_{\rm peak}$, to the in-medium spectral function of two electromagnetic currents (9.48) evaluated at null-momentum $\omega = q$. This in turn produces a peak in the spectrum of thermal photons emitted by the plasma,

$$\frac{dN_\gamma}{d\omega} \sim e^{-\omega/T}\, \chi^{\mu}_{\ \mu}(\omega, T)\,. \tag{9.54}$$

The width of this peak is the width of the meson in the plasma.

The analysis above applies to an infinitely extended plasma at constant temperature. Assuming that these results can be extrapolated to QCD, a crucial question is whether a peak in the photon spectrum could be observed in a heavy ion collision experiment. Natural heavy vector mesons to consider are the J/ψ and the Υ, since these are expected to survive deconfinement. We wish to compare the number of photons coming from these mesons to the number of photons coming from other sources. Accurately calculating the meson contribution would require a precise theoretical understanding of the dynamics of these mesons in the quark–gluon plasma, which at present is not available. Our goal will therefore be to estimate the order of magnitude of this effect with a simple recombination model. The details can be found in Ref. [249], so here we will only describe the result for heavy ion collisions at LHC energies.

The result is summarized in Fig. 9.23, which shows the thermal photon spectrum coming from light quarks, the contribution from J/ψ mesons, and the sum of the two, for a thermal charm mass $M_{\rm charm} = 1.7$ GeV and a J/ψ dissociation temperature $T_{\rm diss} = 1.25T_c$. Although the value of $M_{\rm charm}$ is relatively high, the values of $M_{\rm charm}$ and $T_{\rm diss}$ are within the range commonly considered in the literature. For the charm mass a typical range is $1.3 \leq M_{\rm charm} \leq 1.7$ GeV because of a substantial thermal contribution – see, for example, Ref. [621] and references therein. The value of $T_{\rm diss}$ is far from settled, but a typical range is $T_c \leq T_{\rm diss} \leq 2T_c$ [504, 677, 506, 623, 620, 80, 308, 430, 521, 729, 82]. We have chosen these values for illustrative purposes, since they lead to an order-one enhancement in the spectrum. We emphasize, however, that whether this photon excess manifests itself as a peak, or only as an enhancement smoothly distributed over a broader range of frequencies, depends sensitively on these and other parameters. Qualitatively, the dependence on the main ones is as follows. Decreasing the quark mass decreases the magnitude of the J/ψ contribution. Perhaps surprisingly, higher values of $T_{\rm diss}$

https://doi.org/10.1017/9781009403504.009 Published online by Cambridge University Press

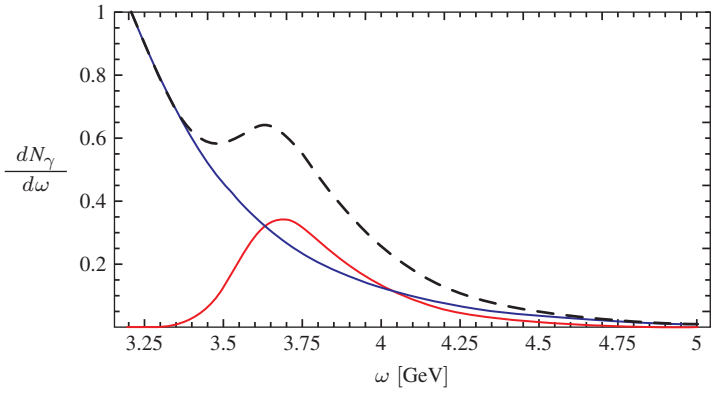

Figure 9.23 Thermal photon spectrum for LHC energies, $T_{\rm diss} = 1.25\,T_c$ and $M_{\rm charm} = 1.7$ GeV. The (arbitrary) normalization is the same for all curves. The continuous, monotonically decreasing, blue curve is the background from light quarks. The continuous red curve is the signal from J/ψ mesons. The dashed black curve is the sum of the two. Figure taken from Ref. [249].

make the peak less sharp. The in-medium width of the J/ψ used in Fig. 9.23 was 100 MeV. Increasing this by a factor of two turns the peak into an enhancement. Crucially, the J/ψ contribution depends quadratically on the $c\bar{c}$ cross-section. Since at RHIC energies this is believed to be ten times smaller than at LHC energies, the enhancement discussed above is presumably unobservable at RHIC.

These considerations show that a precise determination of the enhancement is not possible without a very detailed understanding of the in-medium dynamics of the J/ψ. On the other hand, they also illustrate that there exist reasonable values of the parameters for which this effect yields an order-one enhancement, or even a peak, in the spectrum of thermal photons produced by the quark–gluon plasma. This thermal excess is concentrated at photon energies roughly between 3 and 5 GeV. In this range the number of thermal photons in heavy ion collisions at the LHC is expected to be comparable to or larger than that of photons produced in initial partonic collisions that can be described using perturbative QCD [65]. Thus, we expect the thermal excess above to be observable even in the presence of the pQCD background.

The authors of Ref. [249] also examined the possibility of an analogous effect associated with the Υ meson, in which case $\omega_{\rm peak} \sim 10$ GeV. At these energies the number of thermal photons is very much smaller than that coming from initial partonic collisions, so an observable effect is not expected.

9.6.2 A new mechanism of quark energy loss: Cherenkov emission of mesons

We now turn to another universal prediction that follows from the existence of a subluminal limiting velocity for mesons in the plasma. Consider a highly energetic

https://doi.org/10.1017/9781009403504.009 Published online by Cambridge University Press

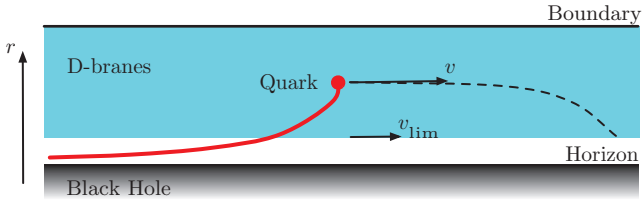

Figure 9.24 D-branes and open string in a black brane geometry. Figure taken from Refs. [255, 256].

quark moving through the plasma. In order to model this we consider a string whose endpoint moves with an arbitrary velocity v at an arbitrary radial position r_q – see Fig. 9.24. Roughly speaking, the interpretation of r_q in the gauge theory is that of the inverse size of the gluon cloud that dresses the quark. This can be seen, for example, by holographically computing the profile of $\langle \mathrm{Tr} F^2(x) \rangle$ around a static quark source dual to a string whose endpoint sits at $r = r_q$ [465].

Two simple observations now lead to the effect that we are interested in. The first one is that the string endpoint is charged under the scalar and vector fields on the branes. In the gauge theory, this corresponds to an effective quark-meson coupling (see Fig. 9.25) of order $e \sim 1/\sqrt{N_c}$. Physically, this can be understood very simply. The fields on the branes describe fluctuations around the equilibrium configuration. The string endpoint pulls on the branes and therefore excites (i.e. it is charged under) these fields. The branes' tension is of order $1/g_s \sim N_c$, where g_s is the string coupling constant, whereas the string tension is N_c-independent. This means that the deformation of the branes caused by the string is of order $e^2 \sim 1/N_c$. We thus conclude that the dynamics of the "branes + string endpoint" system is (a generalization of) that of classical electrodynamics in a medium in the presence of a fast-moving charge.

The second observation is that the velocity of the quark may exceed the limiting velocity of the mesons, since the redshift at the position of the string endpoint is smaller than that at the bottom of the branes. As in ordinary electrodynamics, if this happens then the string endpoint loses energy by Cherenkov radiating into the fields on the branes. In the gauge theory, this translates into the quark losing energy by Cherenkov radiating scalar and vector quarkonium mesons. The rate of energy loss is set by the square of the coupling, and is therefore of order $1/N_c$.

The quantitative details of the energy lost to Cherenkov radiation of quarkonium mesons by a quark propagating through the $\mathcal{N} = 4$ plasma can be found in [256, 255], so here we will describe only the result. For simplicity, we will assume that the quark moves with constant velocity along a straight line at a constant radial position. In reality, r_q and v will of course decrease with time because of the black hole gravitational pull and the energy loss. However, we will concentrate on the initial part of the trajectory (which is long provided the initial quark energy is

https://doi.org/10.1017/9781009403504.009 Published online by Cambridge University Press

Figure 9.25 Effective quark–meson coupling. Figure taken from Refs. [255, 256].

large), for which r_q and v are approximately constant [294] – see Fig. 9.24. Finally, for illustrative purposes we will focus on the energy radiated into the transverse modes of vector mesons. The result is depicted in Fig. 9.26, and its main qualitative features are as follows. (See Refs. [255, 256] for details.)

As expected, we see that the quark only radiates into meson modes with phase velocity lower than v – those to the right of the dashed, vertical lines in Fig. 9.14. For fixed r_q, the energy loss increases monotonically with v up to the maximum allowed value of v – the local speed of light at r_q. As r_q decreases, the characteristic momentum q_{char} of the modes into which the energy is deposited increases. These modes become increasingly peaked near the bottom of the branes, and the energy loss diverges. However, this mathematical divergence is removed by physical effects we have not taken into account. For example, for sufficiently large q the mesons' wave functions become concentrated on a region whose size is of order the string length, and hence stringy effects become important [336]. Also, as we saw in Section 9.4.2, mesons acquire widths $\Gamma \propto q^2$ at large q [347] and can no longer be treated as well defined quasiparticles. Finally, the approximation of a constant-v, constant-r_q trajectory ceases to be valid whenever the energy loss rate becomes large.

The Cherenkov radiation of quarkonium mesons by quarks depends only on the qualitative features of the dispersion relation of Fig. 9.14, which are universal for all gauge theory plasmas with a dual gravity description. Moreover, as we explained in Section 9.4.3, it is conceivable that they may also hold for QCD mesons such as the J/ψ or the Υ whether or not a string dual of QCD exists. Here we will examine some qualitative consequences of this assumption for heavy ion collision experiments. Since the heavier the meson the more perturbative its properties become, we expect that our conclusions are more likely to be applicable to the charmonium sector than to the bottomonium sector.

An interesting feature of energy loss by Cherenkov radiation of quarkonia is that, unlike other energy loss mechanisms, it is largely independent of the details of the quark excited state, such as the precise features of the gluon cloud around the quark, etc. In the gravity description these details would be encoded in the precise profile of the entire string, but the Cherenkov emission only depends on the trajectory of the string endpoint. This leads to a dramatic simplification which, with the further approximation of rectilinear uniform motion, reduces the parameters controlling the energy loss to two simple ones: the string endpoint velocity v and

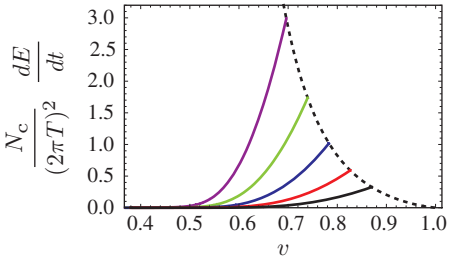

Figure 9.26 Cherenkov energy loss into the transverse mode of vector quarkonium mesons. The continuous curves correspond to increasing values of r_q from left to right. The dotted curve is defined by the endpoints of the constant-r_q curves. Figure taken from Refs. [255, 256].

its radial position r_q. In order to obtain a ballpark estimate of the magnitude of the energy loss, we will assume that in a typical collision quarks are produced with order-one values of r_q (in units of R^2T). Under these circumstances the energy loss is of order unity in units of $(2\pi T)^2/N_c$, which for a temperature range of $T = 200$–$400\,\text{MeV}$ and $N_c = 3$ leads to $dE/dx \approx 2$–$8\,\text{GeV/fm}$. This is is of the same order of magnitude as other mechanisms of energy loss in the plasma; for example, the BDMPS radiative energy loss $dE/dx = \alpha_s C_F \hat{q} L/2$ yields values of $dE/dx = 7$–$40\,\text{GeV/fm}$ for $\hat{q} = 1$–$5\,\text{GeV}^2/\text{fm}$, $\alpha_s = 0.3$ and $L \approx 6\,\text{fm}$. Since our gravity calculation is strictly valid only in the infinite-quark-energy limit (because of the linear trajectory approximation), we expect that our estimate is more likely to be applicable to highly energetic quarks at the LHC than to those at RHIC.

Even if in the quark–gluon plasma the magnitude of Cherenkov energy loss turns out to be subdominant with respect to other mechanisms, its velocity dependence and its geometric features may still make it identifiable. Indeed, this mechanism would only operate for quarks moving at velocities $v > v_{\text{lim}}$, with v_{lim} the limiting velocity of the corresponding quarkonium meson in the plasma. The presence of such a velocity threshold is the defining characteristic of Cherenkov energy loss. The precise velocity at which the mechanism starts to operate may actually be higher than v_{lim} in some cases, since the additional requirement that the energy of the quark be equal or larger than the in-medium mass of the quarkonium meson must also be met.

As illustrated in Fig. 9.27, Cherenkov mesons would be radiated at a characteristic angle $\cos\theta_c = v_{\text{lim}}/v$ with respect to the emitting quark, where v is the velocity of the quark. Taking the gravity result as guidance, v_{lim} could be as low as $v_{\text{lim}} = 0.27$ at the quarkonium dissociation temperature [608, 336], corresponding to an angle as large as $\theta_c \approx 1.30$ rad. This would result in an excess of heavy quarkonium associated with high energy quarks passing through the plasma. Our estimate of the energy loss suggests that the number of emitted J/ψs, for

https://doi.org/10.1017/9781009403504.009 Published online by Cambridge University Press

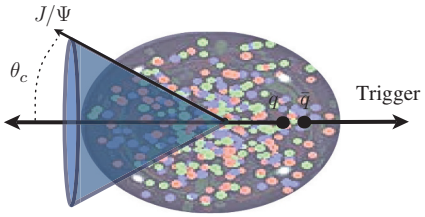

Figure 9.27 The geometry of Cherenkov emission of heavy quarkonium mesons from a highly energetic quark. Figure taken from Ref. [603].

example, could range from one to three per fm. This emission pattern is similar to the emission of sound waves by an energetic parton [245] that we have described in Section 8.3, in that both effects lead to a non-trivial angular structure. One important difference, however, is that the radiated quarkonium mesons would not thermalize and hence would not be part of a hydrodynamic shock wave. The meson emission pattern could be reflected in azimuthal dihadron correlations triggered by a high-p_T hadron. Owing to surface bias, the energetic parton in the triggered direction is hardly modified, while the one propagating in the opposite direction moves through a significant amount of medium, emitting quarkonium mesons. Thus, under the above assumptions, the dihadron distribution with an associated J/ψ would have a ring-like structure peaked at an angle $\theta \approx \pi - \theta_c$. Even if this angular structure were to prove hard to discern, the simpler correlation that in events with a high-p_T hadron there are more J/ψ mesons than in typical events may suffice as a distinctive signature, although further phenomenological modeling is required to establish this.

A final observation is that Cherenkov energy loss also has a non-trivial temperature dependence, since it requires that there are meson-like states in the plasma, and therefore it does not take place at temperatures above the meson dissociation temperature. Similarly, it is reasonable to assume that it does not occur at temperatures below T_c, since in this case we do not expect the meson dispersion relations to become spacelike.[8] Under these circumstances, the Cherenkov mechanism is only effective over a limited range of temperatures $T_c < T < T_{\rm diss}$ which, if $T_{\rm diss} \gtrsim 1.2T_c$ as in Ref. [623], is a narrow interval.

As was pointed out in Ref. [577], a mechanism of energy loss which is confined to a narrow range of temperatures in the vicinity of T_c concentrates the emission of energetic partons to a narrow layer within the collision geometry, and this can have observable consequences. Azimuthally asymmetric particle production at high p_T, say ~ 10 GeV, is parametrized by the same azimuthal Fourier coefficients

[8] This assumption is certainly correct for plasmas with a gravity dual, since the corresponding geometry does not include a black hole horizon if $T < T_c$.

https://doi.org/10.1017/9781009403504.009 Published online by Cambridge University Press

v_2, v_3, ... that at lower p_T are related to hydrodynamic flow. At high p_T, though, these asymmetries originate from jet quenching, and in particular from the fact that in heavy ion collisions with nonzero impact parameter the mean distance through which hard partons traveling in a particular direction relative to the reaction plane must propagate through the medium produced in the collision depends on the angle between the direction of propagation and the reaction plane. Hard partons traveling perpendicular to the reaction plane will, on average, find themselves travelling through the medium for a longer distance (and will therefore lose more energy) than those produced traveling in the reaction plane direction. This effect results in a nonzero v_2 at high p_T. The magnitude of the resulting v_2 will have some sensitivity to the temperature dependence of energy loss. Some authors [577, 356, 822] have found that their models are better able to describe the data if the energy loss occurs only in a narrow range of temperatures near T_c, although others have not needed such a mechanism [499, 500, 145, 498, 626, 146]. Provided that the meson dissociation temperature $T_{\rm diss}$ is not much larger than T_c, the Cherenkov radiation of quarkonium mesons is one such mechanism. The temperature dependence of energy loss is an active area of current research. At the time of writing it remains to be seen whether it favors the Cherenkov radiation of quarkonium mesons as an important energy loss mechanism. It will also be very interesting to look for correlations between J/ψ production and the production and quenching of jets, correlations that go beyond those present in standard perturbative jet fragmentation. This is an investigation that will benefit greatly from the higher production rates for both J/ψ mesons and jets anticipated at the LHC beginning *circa* 2015.

https://doi.org/10.1017/9781009403504.009 Published online by Cambridge University Press